

Next-generation DUV light source technologies for 10nm and below

Ted Cacouris, Greg Rechtsteiner, Will Conley

Cymer LLC, 17075 Thornmint Court, San Diego, CA 92127

ABSTRACT

Multi-patterning techniques with ArF immersion lithography continue to be extended into the 10 and 7 nm nodes. With increasingly challenging process control requirements (CD, overlay, edge placement error), the lithography and patterning tools need to find ways to minimize variation and maintain process margin to achieve high yields. This paper will describe new advances in light source technologies that can regain imaging margins by optimizing light source bandwidth settings in concert with OPC retargeting to take advantage of the contrast improvements^{1,2} afforded by lower bandwidth. In addition to simulation studies reported previously^{3,4}, on-wafer measurements were collected showing the progressive improvements gained with lowering bandwidth on an existing mask as well as reoptimizing a mask to leverage this lower bandwidth setting. To fully leverage this capability, further improvements in bandwidth stability are going to be featured on a new ArF light source along with an integrated solution that allows the bandwidth target to be commanded by scanner recipe. This will allow lithographers to optimize layers that need further improvements in patterning by using lower bandwidth while continuing to run existing layers with standard, 300 fm bandwidth targets. With the introduction of a new DUV light source, this paper will also describe improvements that continue to reduce running costs in an effort to counteract the escalating costs of multi-patterning lithography.

1. INTRODUCTION

Advanced nodes have led to increasing lithography complexity, invoking multi-patterning techniques and designs for manufacturability, including source-mask optimization (SMO) to address the optical proximity challenges that emanate from extending DUV lithography below 10nm. As a result, process windows continue to shrink and require increasingly better process control with sufficient margin to lead to high yields to support the cost-per-bit curve promised by node extensions. While lithography tool developments have helped drive the cost-per-wafer economics with higher throughputs and better CD control for high yields, further improvements can be attained by optimizing light source contributions to patterning. One of the key light source attributes, bandwidth, has become an increasingly important parameter that can help affect patterning quality (Figure 1): improving its stability reduces its contribution to CD variation, while changing the target bandwidth can modulate imaging contrast that can be taken advantage of in optimizing optical proximity corrections (OPC).

2. IMPACT OF HIGHER BANDWIDTH STABILITY

The impact of bandwidth variation on imaging, specifically CD variation, was previously studied through simulations, since experimental studies can be difficult to extract the contribution of bandwidth vs. a multitude of other contributors to this result. Based on these studies, there was a straightforward relationship between bandwidth stability and CD uniformity, consistent with expectations. Of particular interest was the magnitude of the relationship between these two parameters, and, as expected, its increasing importance with more advanced nodes, as represented by CD through pitch simulations (Figure 2).

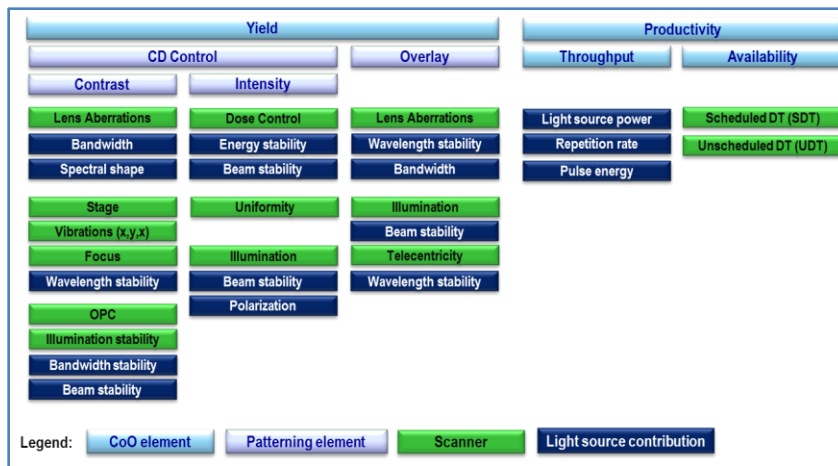


Figure 1 - Light source contributions to key lithography parameters

More recently, these simulations were supplanted with detailed on-wafer studies; based on the modeled relationship between bandwidth stability and CD uniformity, an extensive data sampling plan was prescribed to tease out this relationship relative to other contributors of CD variation. Improvements in the light source bandwidth stability on the latest-generation light sources, such as Cymer's XLR 700ix ArF immersion light source, have demonstrated a reduction in wafer-to-wafer bandwidth variation to the point of eliminating bandwidth as a contributor to CD variation across lots. Direct comparisons between two generations of bandwidth stability have been possible by turning on or off the algorithmic controls that enable improved stability on a specific system, eliminating contributions from tool-to-tool variations.

While improvements in wafer-to-wafer performance have been important to maintain as much process margin as possible, improvements in bandwidth stability intra-wafer can have a similar impact to within-wafer CD uniformity. Similarly, stable bandwidth across an exposure field can help reduce bandwidth contributions to intra-field CD uniformity, contributing to an increased process margin and wafer quality. The technology behind such light source improvements has been based on a unique attribute of the Cymer light sources, wherein bandwidth can be modulated by electronic means. This patented technology leverages the characteristic that as each light pulse develops in the master oscillator (MO) chamber (of a dual-chamber system), it results in a temporal bandwidth distribution which can be selectively amplified by the power ring amplifier (PRA)

chamber by simply adjusting the timing when the PRA chamber fires relative to the MO chamber. The control system can thus provide pulse-to-pulse closed-loop control to maintain high bandwidth stability since it requires no moving parts to achieve this result. The next-generation light source, the XLR 800ix, achieves such high bandwidth stability and dramatically reduces the impact of bandwidth on CD variation.

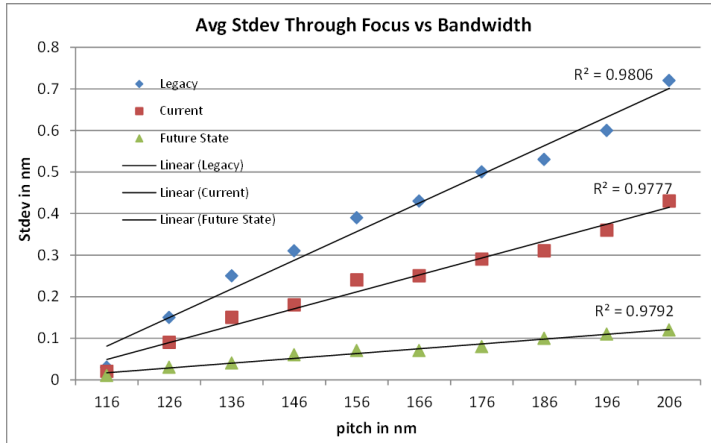


Figure 2 - Simulated CD through pitch variation as a function of bandwidth variation

Figure 3 shows the E95 bandwidth distribution within field and across wafer for three generations of light sources where bandwidth stability is improved progressively from the XLR 600ix to the XLR 700ix and the XLR 800ix models.

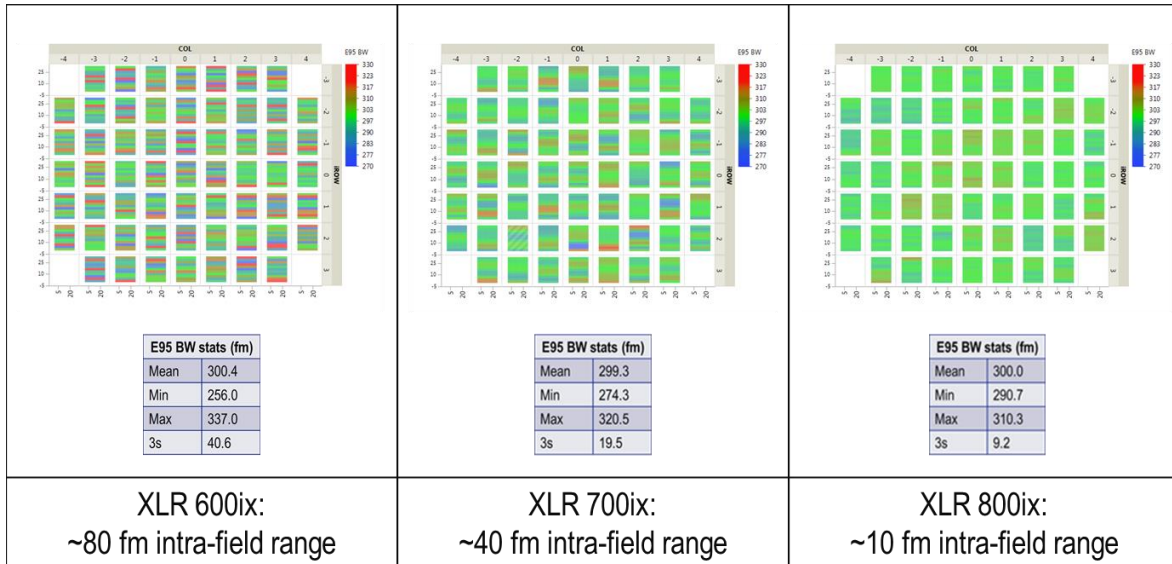


Figure 3 - E95 bandwidth distribution within wafer and intra-field across 3 generations of light source bandwidth control technologies. Full scale color map ranges from 270 to 330nm E95 bandwidth for all three maps.

Using experimental techniques to extract the bandwidth vs. CD response on typical 14nm structures, wafer and field maps can be generated to show the direct impact of improving bandwidth stability on CD uniformity. This translation is depicted in Figure 4 where

progressive improvements in bandwidth stability from one laser model to the next show dramatic improvements in CD uniformity.

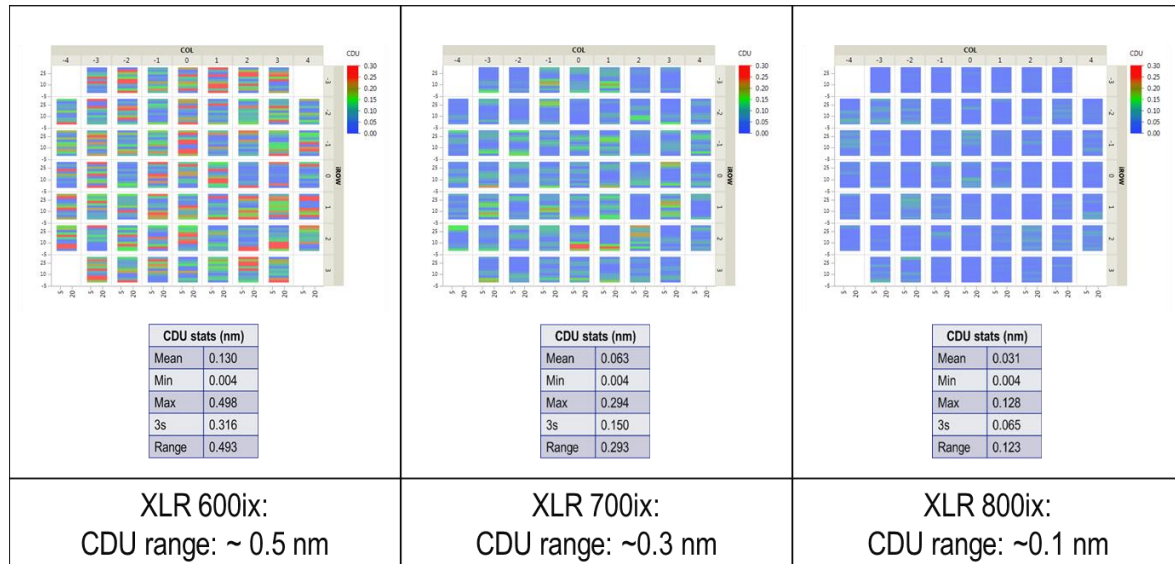


Figure 4 - CD uniformity due to bandwidth variation based on data from Figure 3.

3. PROCESS WINDOW IMPROVEMENTS WITH LOW BANDWIDTH

Since the introduction of ArF immersion light sources, the target bandwidth has been fixed at 300fm, with no change in this parameter as the scanner numerical aperture (NA) has been fixed around 1.35. However, recent studies (simulations) have shown that additional improvements can be attained in addressing hot spots through source optimization at lower bandwidth. Based on these studies, on-wafer experiments were performed⁵ to directly compare nominal vs. low bandwidth exposure conditions. Figure 5 shows an example of self-aligned, quadruple patterning blocks exposed under nominal, 300fm E95 bandwidth vs. the same patterns exposed using source-optimized, 200fm bandwidth. The process window improvement is significant and demonstrates that certain patterning applications can benefit from using bandwidth as an additional optimization knob.

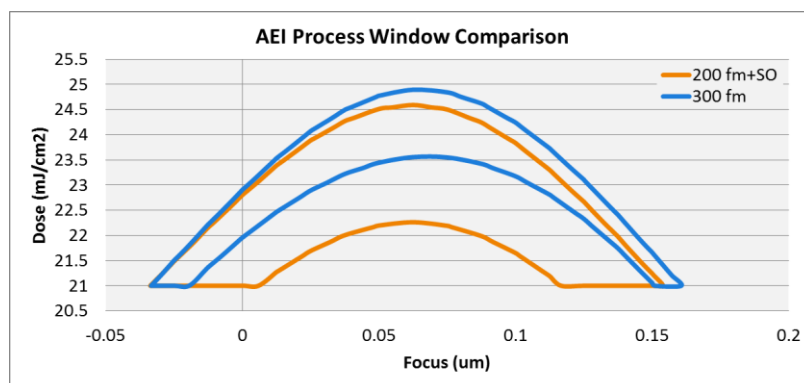


Figure 5 - Process window comparison between standard, 300fm E95 bandwidth and source-optimized 200fm bandwidth on self-aligned, quadruple patterning blocks (from ref. 5).

Similarly, on-wafer experiments were performed⁵ on self-aligned, double patterning features including blocks (with positive-tone develop), comparing nominal, 300 fm bandwidth exposure vs. 200 fm with source optimization, and revealed a notable improvement in exposure latitude as well as a gain in DOF (Figure 6).

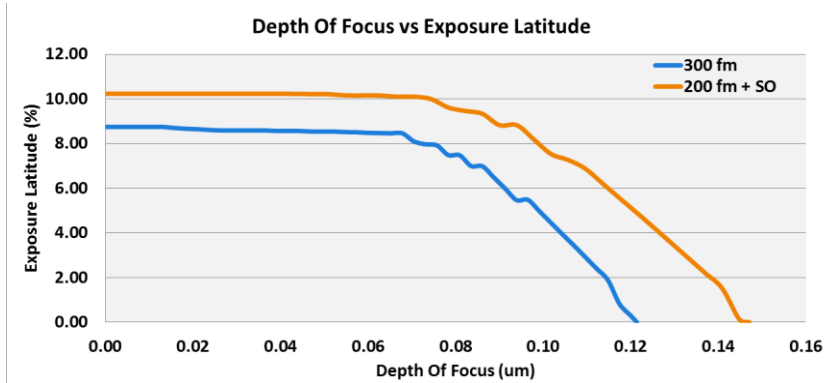


Figure 6 - Exposure latitude (EL) vs. DOF on self-aligned, double patterning + blocks features under nominal, 300 fm E95 bandwidth and source-optimized, 200 fm bandwidth exposure (from ref. 5).

Results such as these described here support a consistent theme where additional process margins can be gained for certain patterns and layers, by simply retargeting the exposure bandwidth with an optimized source, even if the mask itself is not re-optimized. For this reason, the next-generation ArF immersion light source from Cymer, the XLR 800ix, will provide such flexibility in selecting lower bandwidths, in concert with scanner recipe control in order to enable layer-specific bandwidth conditions. Such a configuration will allow the lithographers to identify layers with narrow process windows that could benefit from lower bandwidth and apply these solutions to those layers as needed, while continuing to process layers developed under nominal conditions without interruption.

4. FURTHER IMPROVEMENTS IN COST-OF-OWNERSHIP

While technology extensions are enabling improvements in patterning fidelity, there is still a continuing need to drive running costs down from the equipment perspective. With the introduction of a new DUV light source that provides more stable and tunable bandwidth (Cymer's XLR 800ix), additional enhancements are also being included that enable higher availability and productivity to support an overall cost-of-ownership (CoO) reduction. Key among these improvements is new technology that extends the interval between planned maintenance events by > 30%.

Current, state-of-the-art ArF immersion light sources have a maintenance interval that is largely driven by the life time of the excimer discharge chambers, which typically need replacement at an interval of a year or less, depending on utilization. Improvements to extend the useful life of these chambers have been elusive until recently, where a significant breakthrough in materials optimization within the discharge chamber have enabled a >30% increase in useful life (Figure 7). This improvement directly translates to an increase in availability by an equivalent ratio, enabling higher productivity of the leading-edge, ArF immersion lithography equipment.

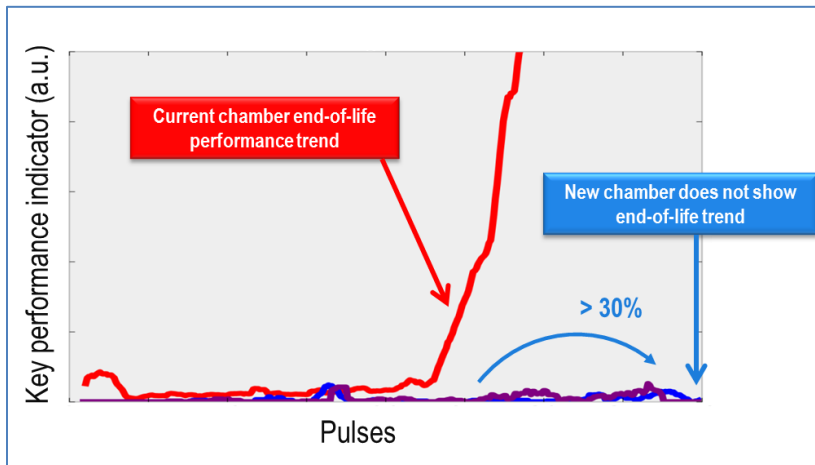


Figure 7 - Current vs. new excimer discharge chamber performance trend vs. life time, measured in pulses.

References

- [1] P. Alagna et al., "Optimum ArFi laser bandwidth for 10nm node logic imaging performance," Proc. SPIE 2015, Optical Microlithography XXVIII, 942609 (2015)
- [2] P. Alagna et al., "Lower bandwidth and its impact on the patterning performance," Proc. SPIE 9780, Optical Microlithography XXIX, 978008 (2016).
- [3] W. Conley et al., "Impact of bandwidth on contrast sensitive structures for low k_1 lithography," Proc. SPIE 2015, Optical Microlithography XXVIII, 942607 (2015)
- [4] W. Conley et al., "Impact of bandwidth variation on OPC model accuracy," Proc. SPIE 9780, Optical Microlithography XXIX, 9780K (2016).
- [5] P. Alagna, et al., "Image contrast enhancement of multiple patterning features through lower light source bandwidth," Proc. SPIE 2017, Optical Microlithography XXX (2017).

The Impact of Lower Light Source Bandwidth on sub-10 nm Process Node Features

Will Conley^a, Paolo Alagna^b, Jason Shieh^c, Simon Hsieh^d,
Tsann-Bim Chiou^c, Stephen Hsu^e, Greg Rechtsteiner^a

^a Cymer LLC, San Diego, CA USA

^b Cymer LLC, Leuven, Belgium

^c ASML TDC, Hsinchu, Taiwan

^d Cymer LLC, Hsinchu, Taiwan

^e ASML Brion, San Jose, CA USA

ABSTRACT

Over the years, lithography engineers continue to focus on CD control, overlay and process capability to meet current node requirements for yield and device performance. Use of ArFi lithography for advanced process nodes demands challenging patterning budget improvements in the range of 1/10 nm especially for interconnect layers.⁽¹⁾ Previous experimental and simulation based investigations into the effects of light source bandwidth on imaging performance have provided the foundation for this work.⁽²⁻⁶⁾ The goal from the light source manufacturer is to further enable capability and reduce variation through a number of parameters.⁽⁷⁻¹⁰⁾

In this study, the authors focus on the increase in image contrast that Source Mask Optimization (SMO) and Optical Proximity Correction (OPC) models deliver when comparing 300 fm and 200 fm light source E95% bandwidth. Using test constructs that follow current N7 / N5 ground rules and multiple pattern deconstruction rules, improvements in exposure latitude (EL), critical dimension (CD) and mask error enhancement factor (MEEF) performance are observed when SMO and OPC are optimized for 200 fm light source bandwidth when compared with the standard 300 fm bandwidth. New SMO-OPC flows will be proposed that users can follow to maximize process benefit. The predicted responses will be compared with the experimental on wafer responses of 7 nm features to lower light source bandwidth.

1. MOTIVATION

Excimer laser bandwidth, specifically E95%, can be seen as a finite oscillation (at decreased intensity) of the central wavelength (figure 1). From basic optical theory, there is a tight correlation between wavelength change and lens aberration response.⁽⁹⁾ In an ideal scenario such variation must be kept as close to zero as possible. In practice, lenses used in the fabrication of the ArF immersion tools are highly chromatic, meaning that small wavelength shifts can cause large focus variation mainly due to chromatic aberration (defined as the longitudinal variation of focus, or image position, with wavelength). Noting that the image formation is the result of the superposition of the image intensities of each of the contributing wavelengths, it can be understood why, in a finite bandwidth domain, the image superposition leads to a focus blur. The amount of this blur is directly proportional to the range of wavelengths sampled.

A reduction in E95% bandwidth directly brings a reduction of the imaging blur enhancing contrast as direct consequence. Therefore, the laser bandwidth has a wide influence on many of the lithography key performance indicators: process window, CD Uniformity, MEEF, OPC validity, etc.

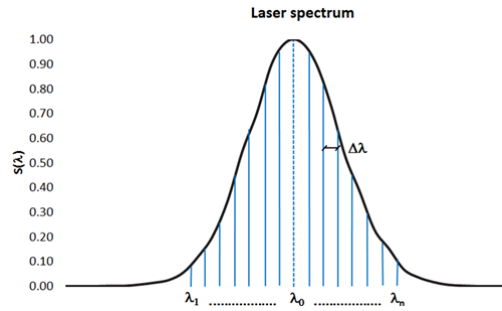


Figure 1: Schematic of finite laser bandwidth

2. LOGIC HOTSPOTS - PREVIOUS STUDIES

2.1 N10 Metal 1 Logic Features

Data from previous studies is shown in figure 2. ^(11,12) The response of the first split of a LELE process was characterized. Changes in the KPIs as function of bandwidth were analyzed on the five different features reported after litho (ADI). The process window analysis was performed on two FEM (Focus Exposure Matrix) wafers at each bandwidth condition (300 fm nominal and 200 fm), with the dose and focus centered at the anchor feature (pitch 96 nm CD 39nm) conditions. Fifty nanometer focus steps and 0.5 mJ/cm² dose steps were used. In general, an increase in exposure latitude is demonstrated when lower bandwidth is used.

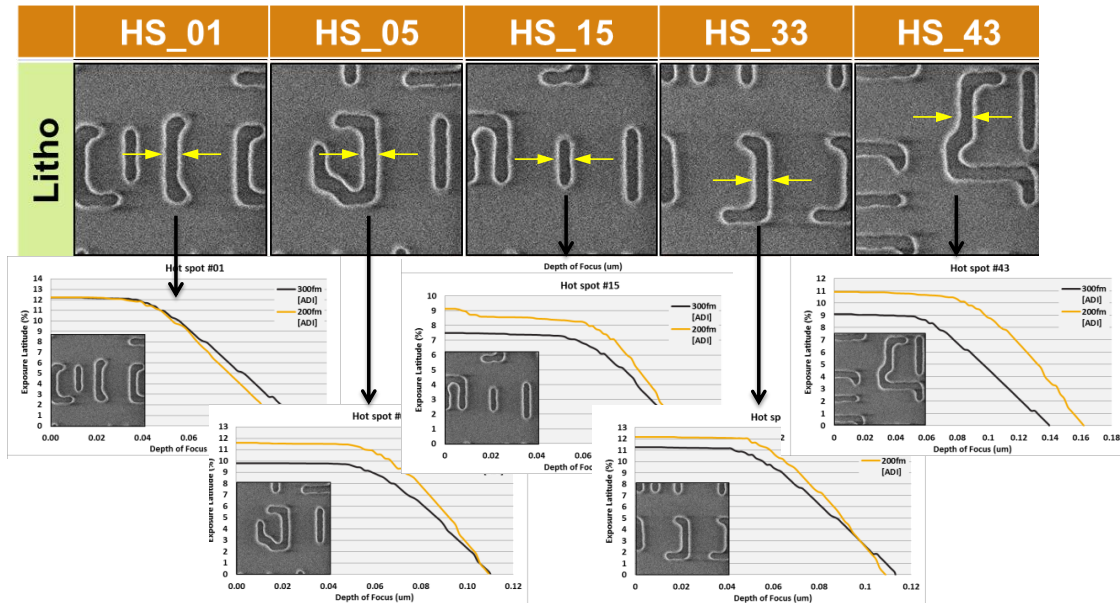


Figure 2: Top SEMs of HS1-43 and associated process windows

3. INVESTIGATING IMAGING PERFORMANCE

3.1 Test Case and Methodology

For this study, E95% bandwidth is a variable that can be adjusted in the machine setup GUI in the Brion Tachyon™ product, which is highlighted in figure 3 below. In this case, in the pull down menu, the NXT:

1950i is chosen which contains all the necessary optical files. The NA (numerical aperture) is 1.35 and the E95 bandwidth conditions are as follows: (a) 0.2 pm or 200 fm and a full width half maximum (FWHM) of 0.120 pm, and (b) 0.3 pm or 300 fm and a FWHM of 0.182 pm. The SMO Tachyon standard optimization flow was used¹³ with x-y polarization (DoP of 0.97), the mask is a 6% attenuated PSM using M3D (3D mask calculation) model and the photoresist is an NTD model with an aerial image blue of 8 nm. Figure 4 is the film stack used for this work.

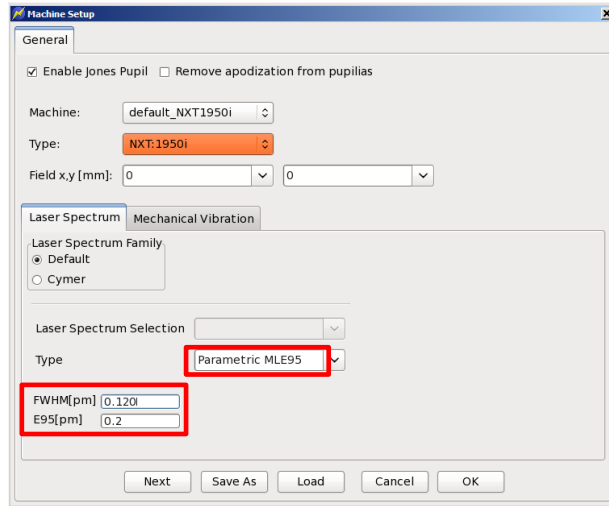


Figure 3: Machine setup GUI in Tachyon

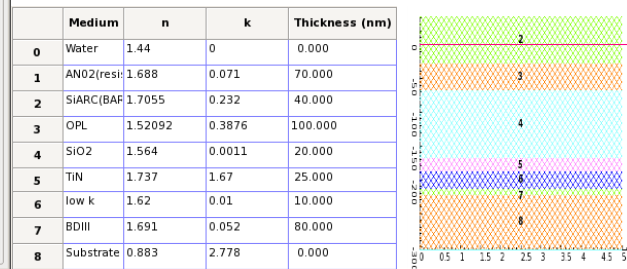


Figure 4: Film stack

3.2 Scenarios and Metrics for comparison

Our investigation focused around 2 scenarios and 2 different layouts which are discussed in section 5.1 and section 5.7. The first scenario is comprised of source and OPC is created with a bandwidth of 300 fm with imaging simulations at 300 fm and 200 fm. In the second scenario is comprised of source and OPC created with a bandwidth of 200 fm with imaging simulations at 200 fm. The maximum exposure latitude, MEEF (mask error enhancement factor) and CDU (critical dimension uniformity) are reported. The CDU is calculated as the RSS from the following settings: mask +/- 0.375 nm, dose +/- 1.5%, and focus +/- 42.5 nm.

4. USE CASES

4.1 M2 Layouts

The test case used in this study is an M2 layer with a post-split pitch of 84 nm. The CD target is 36 nm and the layout is shown in figure 5 pre-OPC.

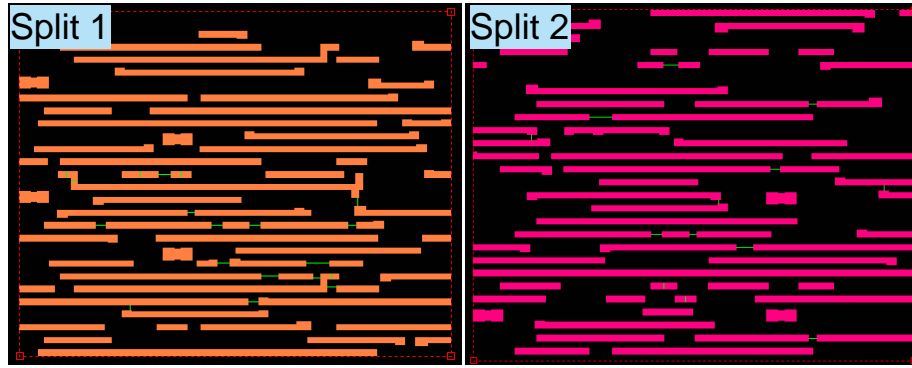


Figure 5: M2 layer P84 after pattern splitting for DPT

4.2 300 fm versus 200 fm SMO – OPC

The results of a change in the light source E95% bandwidth and the creation of a new illumination source are shown in figure 6. The difference between the 300 fm and 200 fm is also shown demonstrating the differences between the two sources.

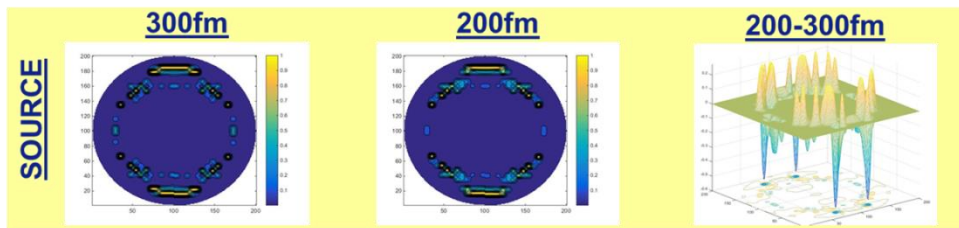


Figure 6: Examples of changes in the source created for 300 fm and 200 fm of E95% bandwidth

As the models used to apply the optimal optical proximity corrections (OPC) should comprehend the light source bandwidth ⁽⁷⁾, therefore a change in bandwidth results in changes in the model solution as shown in Figure 7.

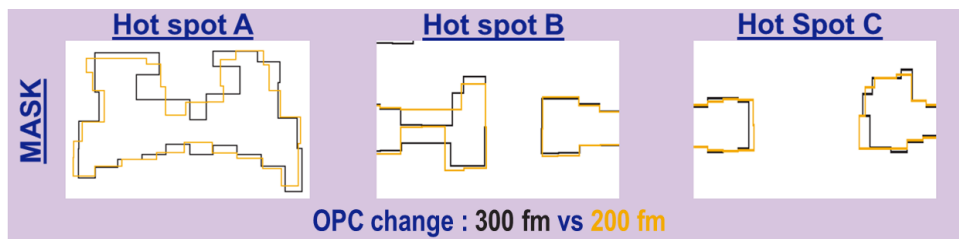


Figure 7: Examples of changes OPC comparing 300 fm and 200 fm of E95% bandwidth

4.3 Hotspots or weak points

Figure 8 is the same GDS as shown in figure 5 but with the specific locations used for all measurements reported based on hotspot detecting using Brion LMC™ ⁽¹⁴⁾.

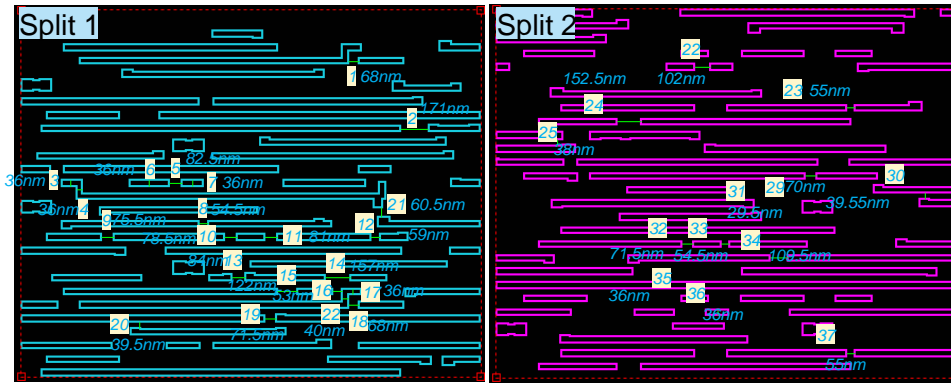


Figure 8: M2 layer P84 after pattern splitting for DPT with weak points highlighted

4.4 M2 Split 1: Exposure Latitude Improvement for 300 fm OPC-SMO with 300 fm imaging and 200fm OPC-SMO with 200 fm imaging

The maximum exposure latitude for each cut line is plotted in figure 9 for each simulated scenario as described in section 4.2. The maximum exposure latitude for 300 fm SMO-OPC with 300 fm imaging along with maximum exposure latitude for 300 fm SMO-OPC with 200 imaging is the plot on left for each metrology marker. On the secondary Y-axis the percent improvement is shown along with a dotted line to guide the eye. An approximate improvement of 2% is demonstrated for this condition.

The plot on the right is the maximum exposure latitude for 300 fm SMO-OPC with 300 fm imaging along with maximum exposure latitude for 200 fm SMO-OPC with 200 imaging for each metrology marker. In this plot a greater response in exposure latitude improvement is demonstrated as indicated on the secondary Y-axis the percent improvement is shown along with a dotted line to guide the eye. An approximate average improvement of 4% is demonstrated for this condition which is a 2x increase over the initial condition.

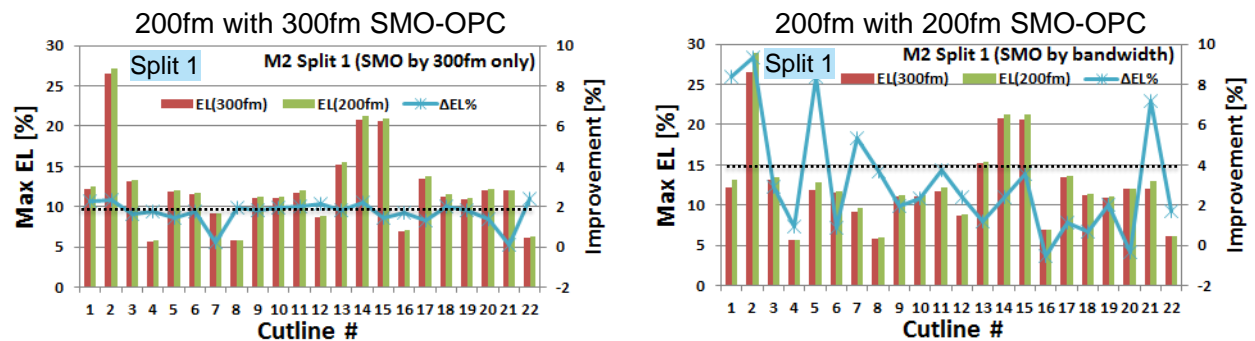


Figure 9: Max % EL for 300 fm SMO-OPC and 200 fm SMO-OPC

Figure 10 is the table created for data comparison for the scenarios discussed in section 4.2. The maximum exposure latitude of 2.37% for scenario 1, split 1 for 300 fm SMO-OPC with 200 fm imaging. The maximum exposure latitude of 9% for scenario 2, split 2 for 200 fm SMO-OPC with 200 fm imaging.

	<u>Scenario 1: Split 1</u>	<u>Scenario 1: Split 2</u>	<u>Scenario 2: Split 1</u>	<u>Scenario 2: Split 2</u>
Max % Increase	300 fm SMO-OPC 200 fm Imaging	300 fm SMO-OPC 200 fm Imaging	200 fm SMO-OPC 200 fm Imaging	200 fm SMO-OPC 200 fm Imaging
M2 (1.5D Case) (EL / CDU / MEEF)	2.37%		9%	

Figure 10: Scenario 1 maximum exposure latitude data summary for split 1

4.5 M2 Split 2: Exposure Latitude Improvement for 200 fm imaging with 300 fm OPC-SMO and 200 fm imaging with 200 fm SMO – OPC

The maximum exposure latitude is plotted in figure 11 for each simulated scenario described in section 4.2 for each cut line. The maximum exposure latitude for 300 fm SMO-OPC with 300 fm imaging along with maximum exposure latitude for 300 fm SMO-OPC with 200 imaging is the plot on left for each metrology marker. On the secondary Y-axis the percent improvement is shown along with a dotted line to guide the eye. An approximate improvement of 1% is demonstrated for this condition.

The plot on the right is the maximum exposure latitude for 300 fm SMO-OPC with 300 fm imaging along with maximum exposure latitude for 200 fm SMO-OPC with 200 imaging for each metrology marker. In this plot a greater response in exposure latitude improvement is demonstrated as indicated on the secondary Y-axis as the percent improvement is shown along with a dotted line to guide the eye. An approximate average improvement of 3% is demonstrated for this condition. It should be noted that cutline 22 had a significant reduction in exposure latitude. Work is in progress to understand the reasons behind this result.

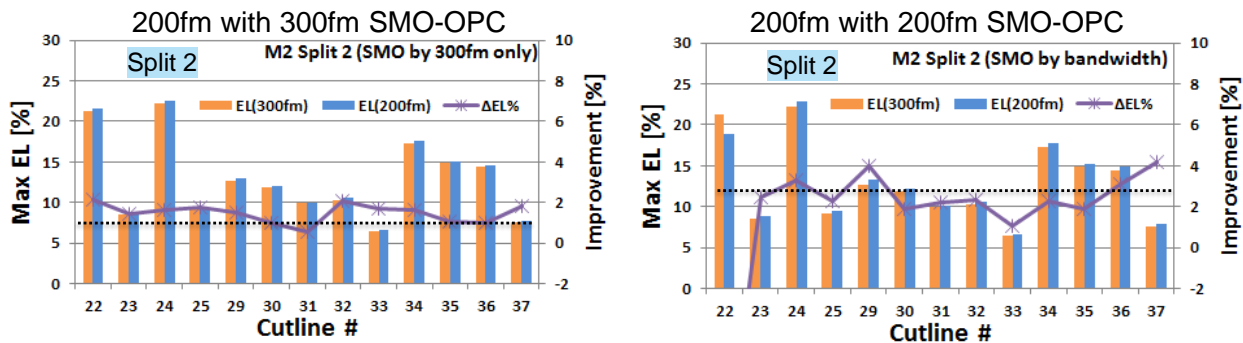


Figure 11: Max % EL for 300 fm SMO-OPC and 200 fm SMO-OPC

Figure 12 is the table created to enter data for comparison for the scenarios discussed in section 4.2. A maximum exposure latitude of 2% for scenario 1, split 2 for 300 fm SMO-OPC with 200 fm imaging. A maximum exposure latitude of 9% for scenario 1, split 2 for 200 fm SMO-OPC with 200 fm imaging.

	<u>Scenario 1: Split 1</u>	<u>Scenario 1: Split 2</u>	<u>Scenario 2: Split 1</u>	<u>Scenario 2: Split 2</u>
Max % Increase	300 fm SMO-OPC 200 fm Imaging	300 fm SMO-OPC 200 fm Imaging	200 fm SMO-OPC 200 fm Imaging	200 fm SMO-OPC 200 fm Imaging
M2 (1.5D Case) (EL / CDU / MEEF)	2.37%	2%	9%	3%

Figure 12: Scenario 1 maximum exposure latitude data summary for split 2

4.6 M2 Split 1: CDU Improvement for 200 fm imaging with 300 fm OPC-SMO and 200 fm imaging with 200 fm SMO – OPC

The CD uniformity for each cut line is calculated and plotted in figure 13 for each simulated scenario described in section 4.2. The CDU in nanometers is plotted on the primary Y-axis and the percent improvement is plotted on the secondary Y-axis for 300 fm SMO-OPC with 300 fm imaging on the left plot. On the secondary Y-axis the percent improvement is shown along with a dotted line to guide the eye. An approximate improvement of 1% is demonstrated for this condition.

The plot on the right is the CD uniformity plotted on the primary Y-axis and the percent improvement is plotted on the secondary Y-axis for 200 fm SMO-OPC with 200 fm imaging on the left plot. On the secondary Y-axis the percent improvement is shown along with a dotted line to guide the eye. An approximate improvement of 5% is demonstrated for this condition. It should be noted that cutline 21 had a significant reduction in exposure latitude. Further work is in progress to understand the reasons behind this reduction.

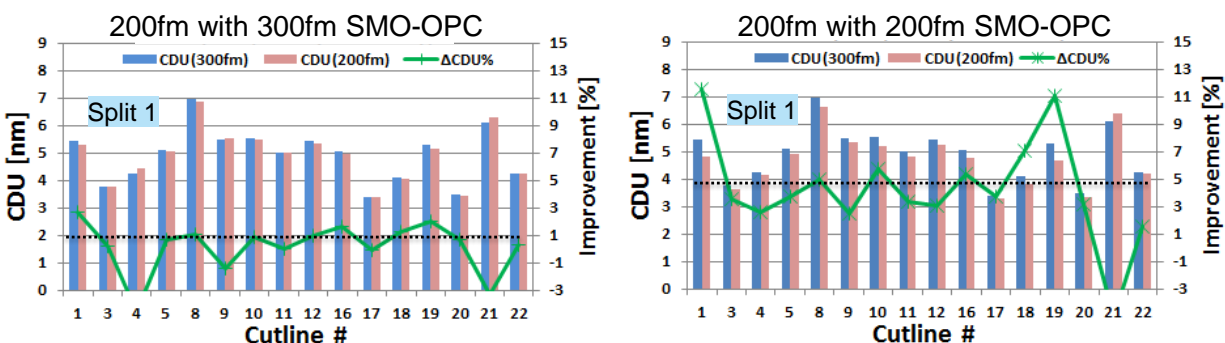


Figure 13: CDU in nm and % improvement

In the figure 14 table, the calculated CDU improvement is 2% for scenario 1, split 1 for 300 fm SMO-OPC with 200 fm imaging. The CDU is improved by 11% for scenario 1, split 1 for 200 fm SMO-OPC with 200 fm imaging.

	Scenario 1: Split 1	Scenario 1: Split 2	Scenario 2: Split 1	Scenario 2: Split 2
Max % Increase	300 fm SMO-OPC 200 fm Imaging	300 fm SMO-OPC 200 fm Imaging	200 fm SMO-OPC 200 fm Imaging	200 fm SMO-OPC 200 fm Imaging
M2 (1.5D Case) (EL / CDU / MEEF)	2.37% / 2% /	2%	9% / 11% /	3%

Figure 14: Scenario 1 CDU data summary for split 1

4.7 M2 Split 1: MEEF Improvement for 200 fm imaging with 300 fm OPC-SMO and 200 fm imaging with 200 fm SMO – OPC

The MEEF is calculated for each cut line and plotted in figure 14 for each simulated scenario described in section 4.2. The MEEF is plotted on the primary Y-axis and the percent improvement is plotted on the secondary Y-axis for 300 fm SMO-OPC with 300 fm imaging on the left plot. On the secondary Y-axis the percent improvement is shown along with a dotted line to guide the eye. An approximate improvement of 1% is demonstrated for this condition.

The plot on the right is MEEF where on the primary Y-axis and the percent improvement is plotted on the secondary Y-axis for 200 fm SMO-OPC with 200 fm imaging on the left plot. On the secondary Y-axis the percent improvement is shown along with a dotted line to guide the eye. An approximate improvement of 5% is demonstrated and is expected based on the improvement in exposure latitude in section 4.4. It should be noted that cutline 21 had an increase in MEEF. Further work is in progress to understand the reasons behind this reduction.

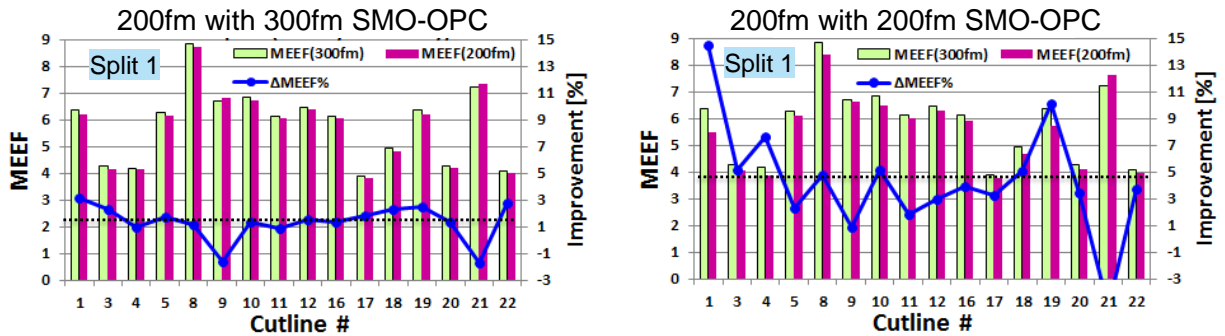


Figure 14: MEEF and % improvement

Figure 15 is the table created to enter data for comparison for the scenarios discussed in section 4.2. The maximum MEEF improvement is 3% for scenario 1, split 1 for 300 fm SMO-OPC with 200 fm imaging. The maximum MEEF is improved by 14% for scenario 1, split 1 for 200 fm SMO-OPC with 200 fm imaging.

	Scenario 1: Split 1	Scenario 1: Split 2	Scenario 2: Split 1	Scenario 2: Split 2
Max % Increase	300 fm SMO-OPC 200 fm Imaging	300 fm SMO-OPC 200 fm Imaging	200 fm SMO-OPC 200 fm Imaging	200 fm SMO-OPC 200 fm Imaging
M2 (1.5D Case) (EL / CDU / MEEF)	2.37% / 2% / 3%	2%	9% / 11% / 14%	3%

Figure 15: Scenario 1 MEEF data summary for split 1

4.8 M1 Cuts

The second test case used in this study is an M1 cut layer. The CD target is 40 nm and the layout is shown in figure 16 pre-OPC.

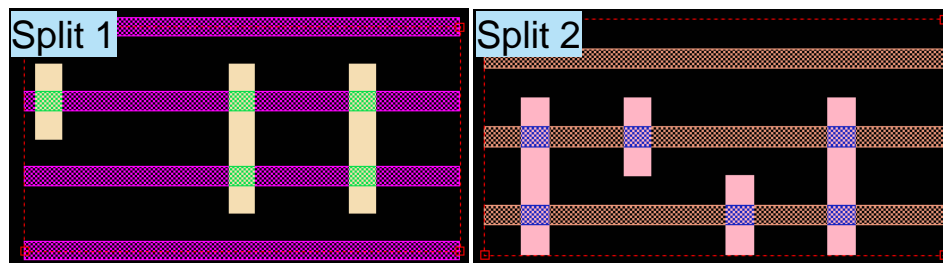


Figure 16: M1 cut layer test case after pattern splitting for DPT

Figure 17 is M1 cut layer post OPC. The assist features, OPC, and the drawn image are shown. The simulated photoresist images are overlaid demonstrating the OPC fit to meet the drawn image. Each

metrology marker is also shown for each split for reference to the data provided in section 5.10. Additionally, the illuminator is shown for the 300 fm and 200 fm case. Differences can be detected at the 12 and 6 o'clock position along with the 9 and 3 o'clock positions.

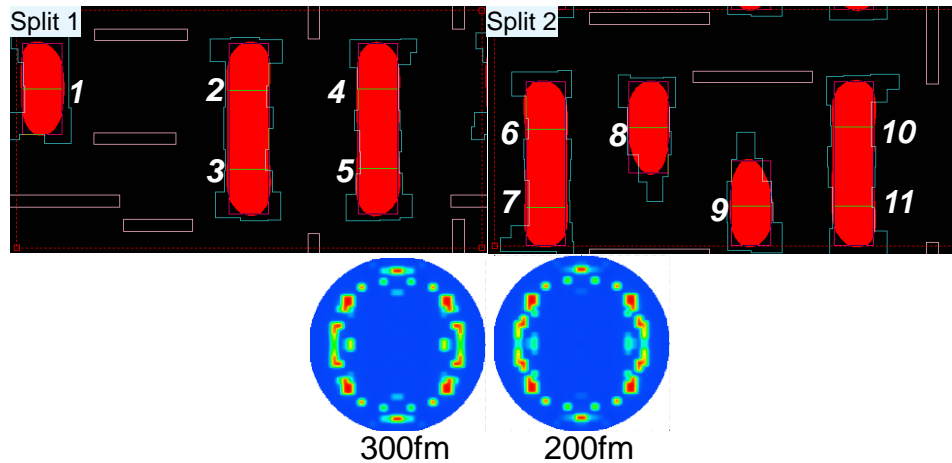


Figure 17: M1 cut layer test case after pattern splitting for DPT

4.9 Exposure Latitude with 300 fm SMO-OPC with 300 fm imaging and 200 fm SMO-OPC with 200 fm imaging

The maximum exposure latitude is plotted in figure 18 for each simulated scenario described in section 5.8 for each cut line. Maximum exposure latitude for 300 fm SMO-OPC with 300 fm imaging along with maximum exposure latitude for 300 fm SMO-OPC with 200 imaging is the plot on left for each metrology marker. On the secondary Y-axis the percent improvement is shown along with a dotted line to guide the eye. An approximate improvement of 2% is demonstrated for this condition.

The plot on the right the maximum exposure latitude for 300 fm SMO-OPC with 300 fm imaging along with maximum exposure latitude for 200 fm SMO-OPC with 200 imaging for each metrology marker. In this plot a greater response in the improvement in exposure latitude is demonstrated as indicated from on the secondary Y-axis the percent improvement is shown along with a dotted line to guide the eye. An approximate average improvement of 8% is demonstrated for this condition which is a 4x increase over the initial condition.

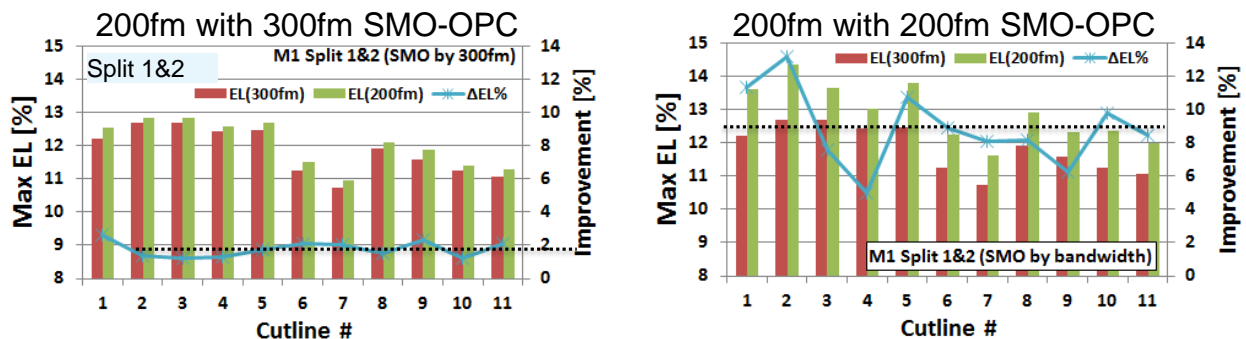


Figure 18: Max % EL for 300 fm SMO-OPC and 200 fm SMO-OPC

Figure 19 is the table created to enter data for comparison for the scenarios discussed in section 5.8. The maximum EL improvement is 2.2% for scenario 1, split 1 and 2 for 300 fm SMO-OPC with 200 fm imaging. The maximum EL is improved by 13% for scenario 2 split 1 and 2 for 200 fm SMO-OPC with 200 fm imaging.

Max % Increase	Scenario 1: Split 1 300 fm SMO-OPC 200 fm Imaging	Scenario 1: Split 2 300 fm SMO-OPC 200 fm Imaging	Scenario 2: Split 1 200 fm SMO-OPC 200 fm Imaging	Scenario 2: Split 2 200 fm SMO-OPC 200 fm Imaging
M2 (1.5D Case) (EL / CDU / MEEF)	2.37% / 2% / 3%	2%	9% / 11% / 14%	3%
Metal Cuts (EL)	2.2%		13%	

Figure 19: Scenario 1 and 2 summary for split 1 and 2

5. EXPERIMENTAL DATA

5.1 Self Aligned Double Patterning + Blocks (PTD) Process Flow

Experimental data was collected from the patterning flow PTD (positive tone develop) blocks on the SADP (self-aligned double patterning) flow shown in Figure 20.⁽¹⁵⁾

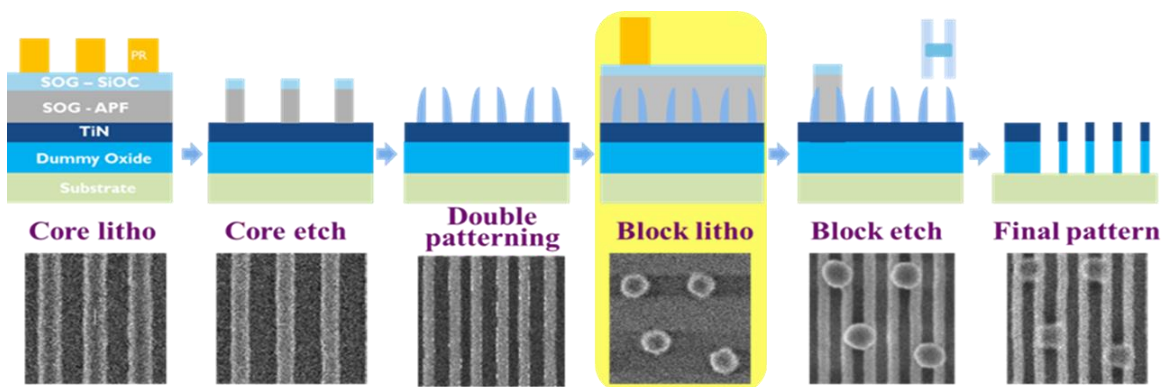


Figure 20: SADP+Blocks flow used in experimental work

The blocks features which were considered in this experiment are characterized by a matrix of round pillars with a target CD on wafer of 51 nm. From a design prospective, the matrix is generated by repeating the same four-OPC-fingerprint multiple times.

5.2 Self Aligned Double Patterning + Blocks (PTD) Process Capability

Both theory and previous experimental activities indicate that tuning only the light source bandwidth increases imaging contrast and can provide increased exposure latitude (EL) with limited degradation in the depth of focus.⁽¹¹⁾ In this study, it has been demonstrated that working in a semi-optimized-regime (only source optimized) it is possible to maintain the optimal response in terms of EL increase while correcting for any loss in DOF, or in cases like the ADI Blocks an increase, as shown in Figure 21.

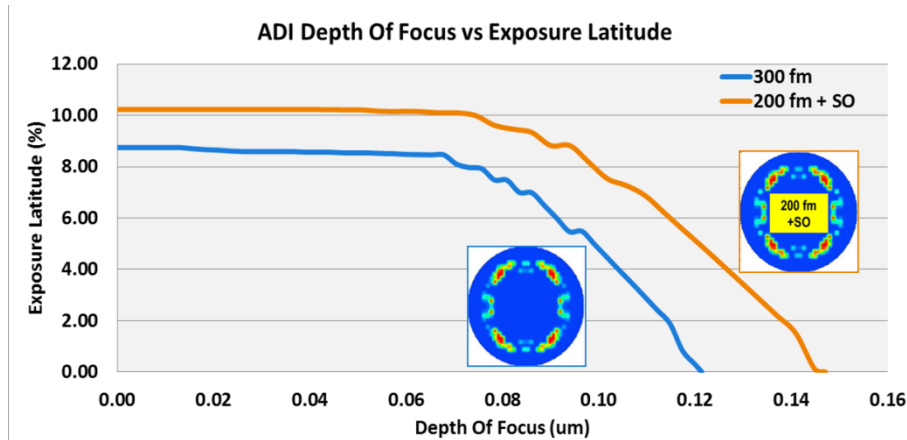


Figure 21: Exposure latitude vs Depth of Focus plot : +20% DOF (+30 nm) and +11% EL (+1 %)

6. CONCLUSIONS & FUTURE WORK

Figure 22 below is the completed table with the experimental data added for SADP blocks demonstrating the increase in EL and DoF for this case. This provides further evidence that the incorporation of bandwidth into the optimization of “the system” has been demonstrated to provide further process value through increased exposure latitude, improvement in CDU and reduction of MEEF. A methodology for the creation of new source and OPC was demonstrated in the Tachyon system. Simulated and experimental data have been provided indicating that further optimization and or design tradeoffs could be needed to ensure that the entire design benefits from this capability are achieved. As shown in the experimental data, reduced bandwidth can be combined with full Source Mask Optimization (SMO) to provide additional process benefits while maintaining the initial mask created at the nominal bandwidth. Further work is in progress to verify the benefit for other types of designs.

Max % Increase	Reference:	Scenario 1: Split 1 300 fm SMO-OPC 200 fm Imaging	Scenario 1: Split 2 300 fm SMO-OPC 200 fm Imaging	Scenario 2: Split 1 200 fm SMO-OPC 200 fm Imaging	Scenario 2: Split 2 200 fm SMO-OPC 200 fm Imaging
M2 (1.5D Case) (EL / CDU / MEEF)		2.37% / 2% / 3%	2%	9% / 11% / 14%	3%
Metal Cuts (EL)		2.2%		13%	
SADP BLOCKS (Exp: EL, DoF)	8.5% / 120 nm			10.2% / 145 nm 300 fm OPC	

Figure 22: Scenario 2 split 1 increase in process capability vs. the reference and final summary

7. ACKNOWLEDGEMENTS

The Authors would like to thank our Colleagues in the Cymer Applications team, the Brion Model and SMO teams, Shao-Ying Huang at Brion Taiwan and the ASML TDC Management for their support.

8. REFERENCES

1. 2015 International Technology Roadmap for Semiconductors (ITRS);
http://www.semiconductors.org/main/2015_international_technology_roadmap_for_semiconductors_itrs/
2. W. Conley et al., "Impact of bandwidth on contrast sensitive structures for low k1 lithography" , Proc. SPIE 9426, Optical Microlithography XXVIII, 942607 (2015).
3. W. Conley et al., "Impact of bandwidth variation on OPC model accuracy" , Proc. SPIE 9780, Optical Microlithography XXIX, 9780K (2016).
4. P. Alagna et al., "Optimum ArFi Laser Bandwidth for 10nm Node Logic Imaging Performance", Proc. SPIE 9525, Optical Microlithography XXVIII, 952508 (2015).
5. P. Alagna et al., "Lower bandwidth and its impact on the patterning performance", Proc. SPIE 9780, Optical Microlithography XXIX, 978008 (2016).
6. P. Alagna et al., "Image contrast enhancement of multiple patterning features through lower light source bandwidth", SPIE 2017 (TBD).
7. I. Lalovic et al., Defining a physically-accurate laser bandwidth input for optical proximity correction (OPC) and modeling, Proc. BACUS XXII Photomask Technology Symposium 7122 -62, (2008).
8. P. De Bisschop et al., Impact of finite laser bandwidth on the CD of L/S structures, Journal of Micro / Nanolithography, MEMS and MOEMS (JM3), Vol. 7, No. 3, (2008)
9. M. Smith et al., Modeling and Performance Metrics for Longitudinal Chromatic Aberrations, Focus-drilling, and Z-noise; Exploring excimer laser pulse-spectra," Proc. SPIE Optical Microlithography XX 6520 -127 (2007)
10. U. Iessi et al., Laser bandwidth effect on overlay budget and imaging for the 45 nm and 32nm technology nodes with immersion lithography, Proc. SPIE Optical Microlithography XXIII 7640 (2010).
11. P. Alagna et al., "Optimum ArFi laser bandwidth for 10nm node logic imaging performance", Proc. SPIE 2015, Optical Microlithography XXVIII, 9426,09
12. W. Conley et al., "Impact of bandwidth on contrast sensitive structures for low k1 lithography", Proc. SPIE 2015, Optical Microlithography XXVIII, 9426,07
13. https://staticwww.asml.com/doclib/productandservices/TACHYON_SMO_source_and_mask_co-optimization.pdf
14. V. Timoshkov, et al. "Imaging challenges in 20nm and 14nm logic nodes: hot spots performance in Metal 1 layer" Proc. SPIE 8886, 88860N
15. Paolo Alagna et al, Proc SPIE 2017, Optical Microlithography XXX to be published.

Assessment of light source bandwidth impacts on image contrast enhancement using Process Window Discovery

Paolo Alagna^a, Greg Rechtsteiner^b, Will Conley^b, Andrew Cross^c, Kaushik Sah^c, and Sandip Halder^d

a) Cymer LLC, Kapeldreef 75, 3001 Leuven, Belgium

b) Cymer LLC, 17075 Thornmint Court, San Diego, CA 92127

c) KLA-Tencor, One Technology Drive, Milpitas, California 95035, USA

d) imec, Kapeldreef 75, 3001 Leuven, Belgium

ABSTRACT

The performance requirements of advanced semiconductor technology nodes necessitate the use of complex processing methods that push patterning beyond the physical limits of DUV immersion lithography (ArFi). Specifically, aggressive process window and yield specifications put tight requirements on scanner imaging performance.

Accurate identification of process windows can be accomplished using KLA-Tencor's fixed focus offset conditions and Process window Discovery (PWD) methodology^[1]. The PWD methodology makes use of a modulated wafer layout to enable inspection comparing nominal to modulated conditions. KLA-Tencor's Broadband plasma (BBP) inspection technology is used to compare the nominal conditions to each experimental condition and to identify systematic defects. The identification of systematic defects is enabled by the PWD method by first discovering potential patterns of interest and then generating Nanopoint™ care areas around every occurrence of the patterns of interest. This allows identification of critical systematic structures that may have the same design intent but do not repeat in the same X,Y locations within a device. This approach maximizes the inspection sensitivity on each structure type, accurately identifies the edge of the process window in focus and dose, and enables study of the sensitivity of fixes process offsets (such as light source bandwidth).

In this study, a tunable DUV light source bandwidth technique and the PWD methodology are used to study the light source E95 bandwidth impact on Metal layer features from an imec 10 nm node logic-type test vehicle.

MOTIVATION

To meet the demanding low k1 printing requirements of advanced process nodes, ArFi lithography must identify solutions to significant challenges in patterning. To overcome these challenges, chip makers are using DUV lithography multiple patterning and DTCO techniques that enable device dimensional scaling despite aggressive process window and yield specifications.

The optimal printability for multiple patterning based logic devices is driven by the optimization of the optical proximity correction (OPC) and by complex process factors, such as resist, exposure tool, and mask-related error performance levels. In addition, the DUV light source plays a crucial role as it has been widely demonstrated^[5-9] how changes in the E95 bandwidth can significantly lead to changes in on wafer patterning due image contrast changes.

As demonstrated in previous studies^[2-3], a significant improvement to multiple patterning solutions can be achieved by leveraging light source capabilities. For example, assessments have been made showing the E95 bandwidth control range required to obtain optimal patterning performance on 10 nm process node Metal 1 logic layers (in a LELELE patterning flow, see Figure 1). It has also been shown that logic patterns designed for triple patterning applications (like the one considered in these studies) utilize complex OPC structures thereby increasing the difficulty in predicting changes in Critical Dimension (CD) due to E95 bandwidth when compared to basic line and space^[4].

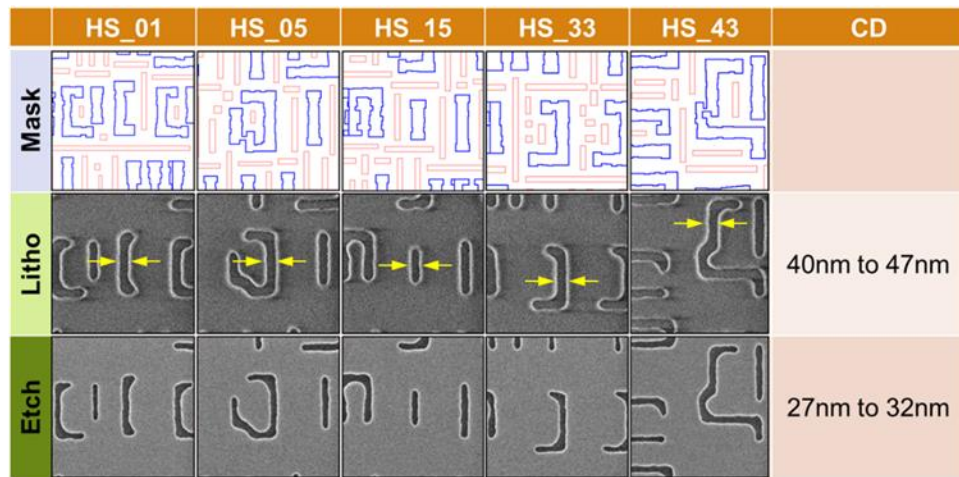


Figure 1. Randomly routed 2D logic structures from imec's 10 nm process M1 layer that are ideal for detecting process variations due to light source bandwidth.

As reported previously^[3], a Process Window (PW) analysis was performed on two FEM (Focus Exposure Matrix) wafers at each bandwidth condition: 300 fm nominal and 200 fm. It is important to note that the studies were performed on masks with OPC models optimized at 300 fm. The results reported in Figure 2 show an increase in the maximum exposure latitude (EL) induced by the higher imaging contrast of lower E95 bandwidth. The distribution observed across the five hot spots can be explained by a combination of factors such as the intrinsic characteristics of the feature and the optical proximity being uncorrected for 200 fm exposure.

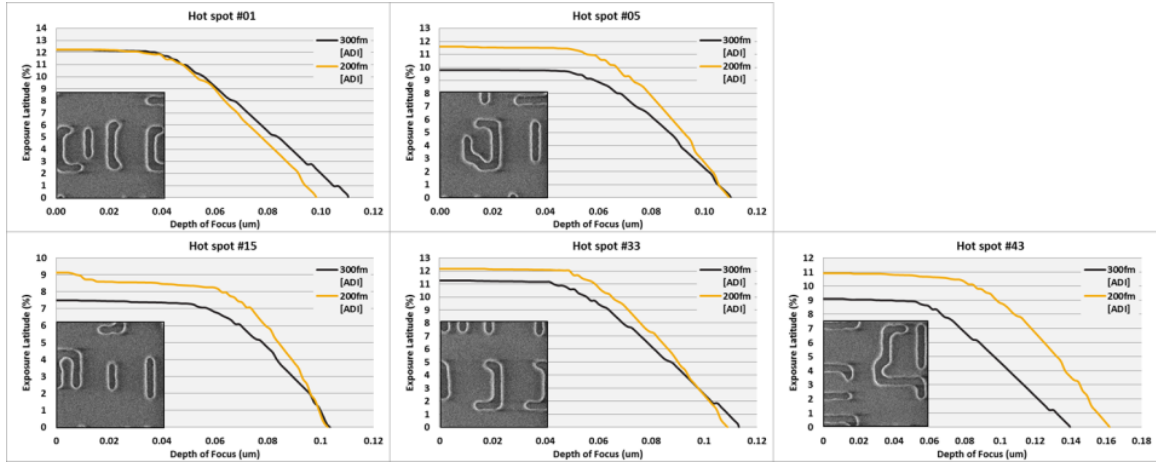


Figure 2. ADI results showing the impact of light source bandwidth on hot spot process window performance.

The work presented this year is a significant extension to this previous work, using a tunable light source bandwidth technique and the PWD methodology to study the light source E95 bandwidth impact on Metal layer features for an imec 10 nm node logic type test vehicle (see Figure 1).

EXPERIMENTAL CONDITIONS

This study probes the E95 bandwidth sensitivity of a 10 nm node dual damascene Metal 1 (M1) layer with a nominal pitch of 48 nm and a nominal trench width of 24 nm as engineered at imec as part of a LELELE triple patterning process. The substrate process stack is shown in Figure 3.

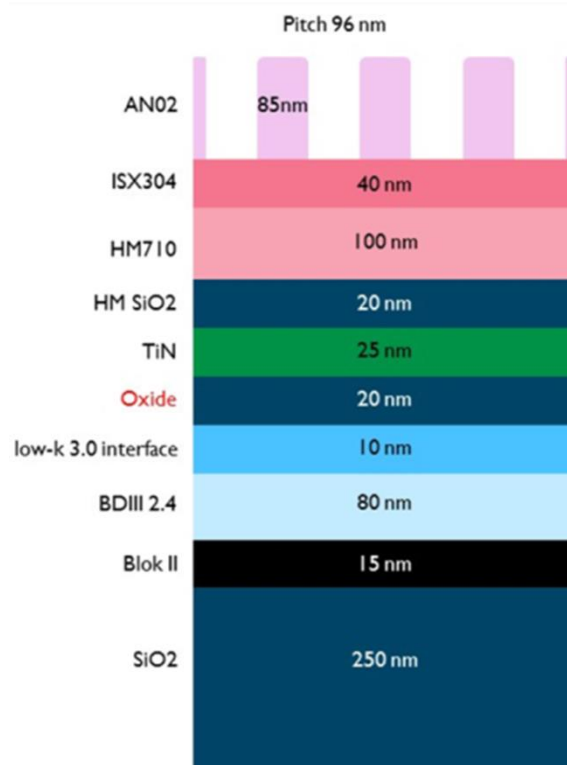


Figure 3. Process stack for the imec M1 layer used in this study.

The target pattern consists of 2D logic type structures which are randomly routed on large areas in the field, which makes this layout ideal to detect process variations within the field and within the wafer. Figure 1 shows a representative example of the type of patterns that are found on this device. The dose to size was selected by targeting the CD for the hot spot features to be between 27 and 32 nm (± 3 nm) at after etch inspection (AEI).

Based on the results from previous studies showing an improvement in PW at 200 fm E95 bandwidth, two types of OPC were generated and placed on a test mask: one for 300 fm bandwidth (nominal) and another for 200 fm bandwidth (extrapolated based on dose offset) as shown in Figure 4. It is important to note that the 200 fm OPC mask feature model does not include optimization of the illumination source; that is, a full SMO-OPC model was not generated. Wafers were exposed at multiple light source E95 bandwidth set points between 200 and 400 fm to assess the patterning response of the nominal and extrapolated OPC conditions.

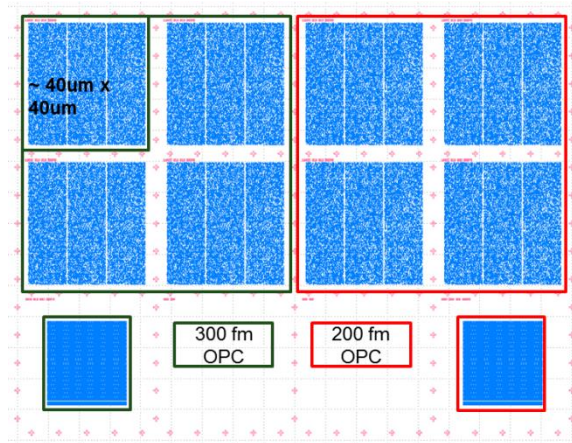


Figure 4. Test mask layout showing the cells with 300 fm and 200 fm bandwidth OPC features.

PROCESS WINDOW DISCOVERY CONDITIONS

The impact of light source bandwidth on the target features was investigated on focus-exposure (FE) modulated layouts and fixed focus offset wafers using the Process Window Discovery (PWD) methodology^[1].

The starting point is a two-pass Process Wafer Qualification inspection. The PWD methodology makes use of a modulated wafer layout to discover hotspots and to define the process window. The layout used is shown in Figure 5, where focus is modulated on the outer columns of the wafer, dose is modulated in the center column of the wafer, and nominal condition columns are printed on each side of these modulated columns.

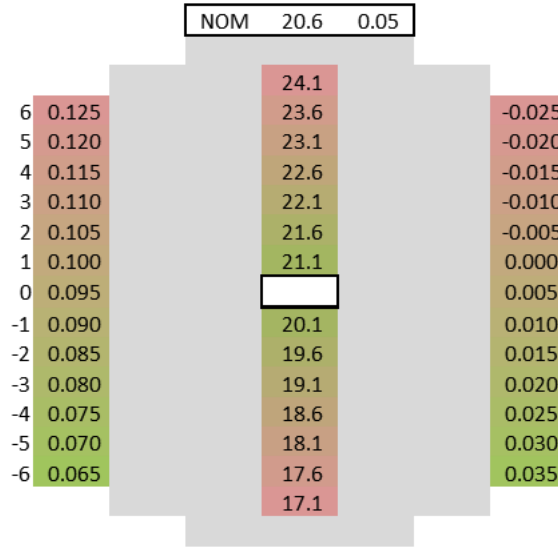


Figure 5. Wafer layout for the nominal bandwidth PWQ exposure condition.

Broadband plasma (BBP) inspection technology is used to compare the nominal conditions to each experimental condition and to identify systematic defects with design enabled inspection. BBP inspection is used to understand the impact of bandwidth, both within the exposure field and across the wafer, as it has good coverage on the wafer without sacrificing sensitivity.

Once the highest priority hotspots are identified and ranked, the second phase of PWD runs the same Nanopoint™ (NP) inspection on wafers that are processed with a uniform offset over a full wafer (i.e. the same condition used for all fields). This offset can be a focus offset, dose offset or, in this case, the DUV light source bandwidth. In this study, the feature set was intentionally limited to a small design area containing a repeating layout of hot spot features (see Figure 6). Even with a small area (< 200 x 200 μm), the optical inspection was completed with excellent results at AEI (post TiN etch).

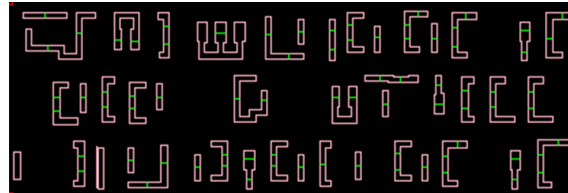


Figure 6. Representative mask clip of the 2D logic patterns found on the M1 layer used for this study.

EXPERIMENTAL RESULTS

For the defect inspection a die-to-die method was used. Due to process variations, differences between dies can be detected by optical defect inspection. Figure 7 shows the excellent correlation between the defect inspection and design for a sample hot spot (HS_15 as shown in Figure 1).



Figure 7. Nominal defect inspection image (left), design clip (middle), and hot spot detected defect inspection image (right).

Process Wafer Discovery wafer inspection

The PWD maps show how defect inspection can help to visualize the impact of light source E95 bandwidth on hot spot process windows. The inspection result shown in Figure 8 is for the nominal 300 fm condition (light source and OPC).

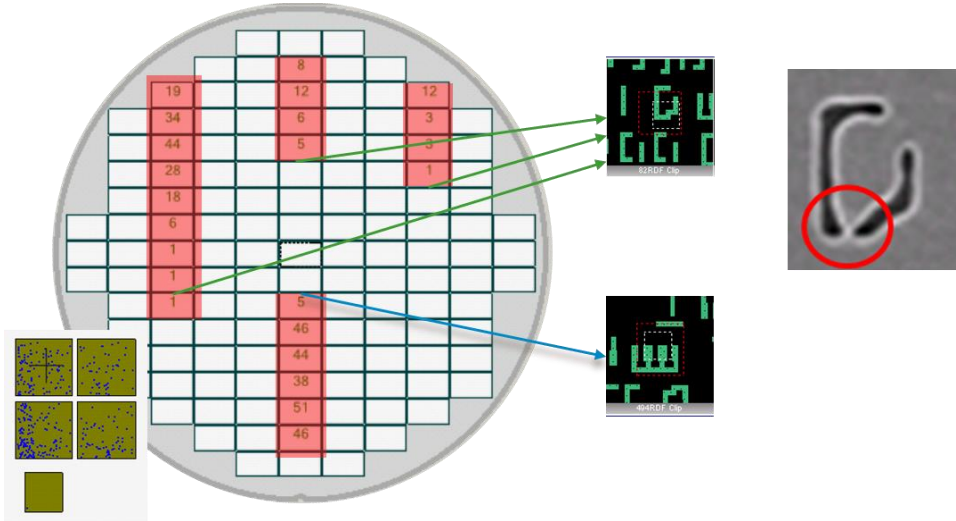


Figure 8. PWD inspection map for the nominal 300 fm bandwidth condition (left) and CD SEM image of key process window limiting hot spot feature (enlarged, right).

The inspection result for 200 fm E95 bandwidth light source exposure and the 200 fm extrapolated OPC features is shown in Figure 9 and indicate a similar response. Representative failure modes for the process window limiting features are shown in the CD SEM images.

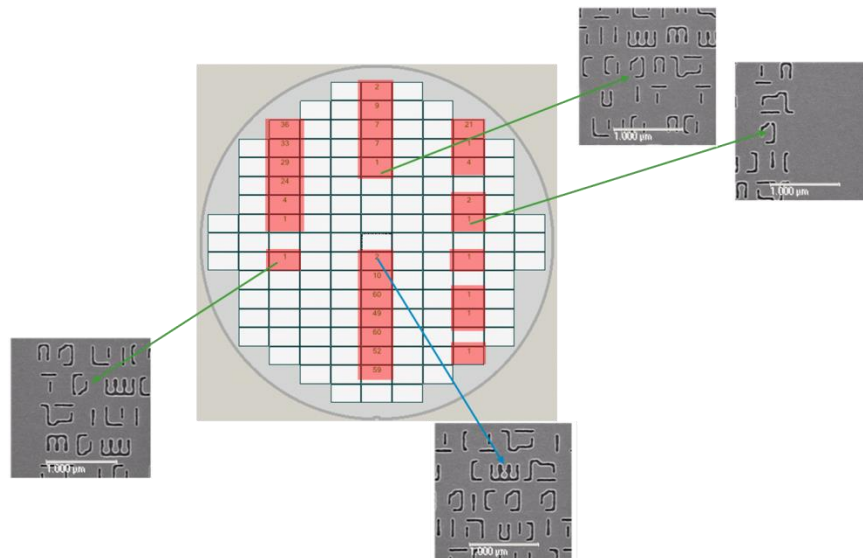


Figure 9. PWD inspection map and key process limiting features for the 200 fm bandwidth and 200 fm OPC condition.

Fixed offset (Uniformity) wafer inspection

The fixed offset (Uniformity) inspection maps further demonstrate how defect inspection can help to visualize the impact of light source E95 bandwidth on hot spot process windows. The inspection result shown in Figure 10 is for the nominal 300 fm condition (light source and OPC).

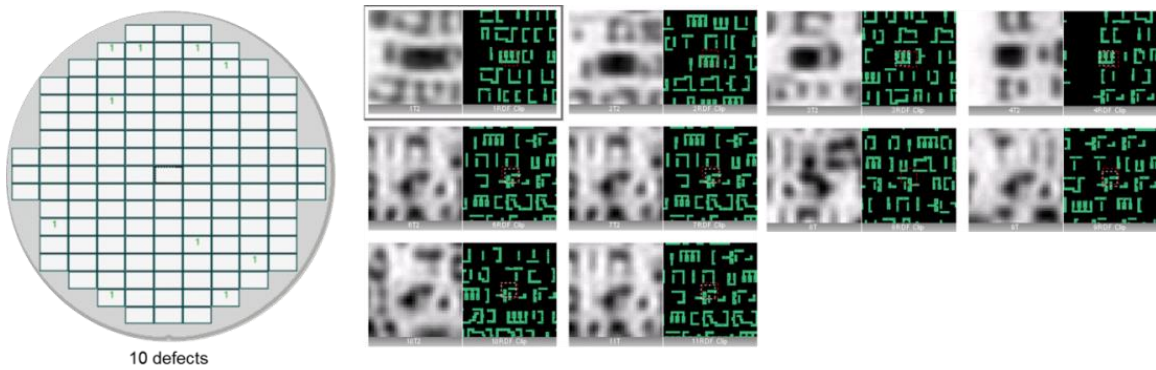


Figure 10. Uniformity wafer inspection map for the nominal 300 fm bandwidth condition (left) and detected defects (right). Note that bridging defects are indicated by the dark polarity.

For the nominal uniformity wafer, no patterning failures are observed for the key process window limiting hot spot. It should be noted that the defects primarily exist at the edge of the wafer, indicating lower margin due to process and/or topography variations.

Analysis of the 200 fm E95 results will be discussed in the next section.

ANALYSIS AND DISCUSSION

Process Wafer Discovery wafers

The defect mode classification for the PWD wafer with nominal OPC at 300 fm light source bandwidth exposure is shown in Figure 11. The process window limiting feature at positive defocus and positive dose is the hot spot HS_05 (also shown in Figures 1 and 8) and is indicated on the design clip. At negative defocus and negative dose, a different feature is the process window limiter; the multiple finger structure as shown on the design clip. For ArFi patterned features like these, the hotspot-types observed in positive defocus and negative defocus can be different due to profile changes in the negative tone resist process. This is clearly demonstrated in Figure 12 showing the different process window limiting features at positive and negative defocus. Previous studies have attributed this difference to profile changes in the NTD resist process at the different defocus extremes^[1].

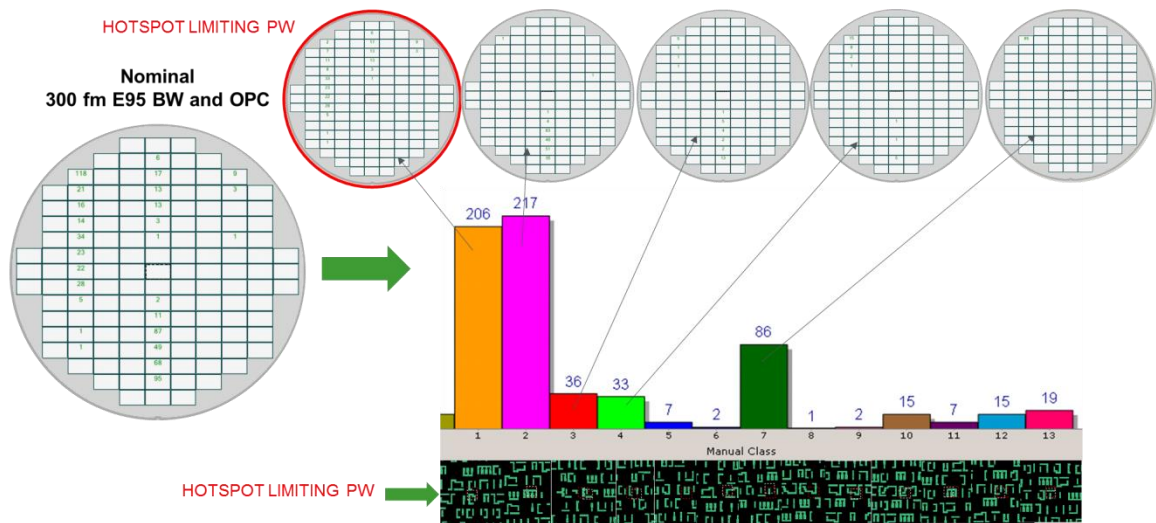


Figure 11. PWD inspection map for the nominal 300 fm bandwidth condition and classification of key process window limiting hot spot features (right).

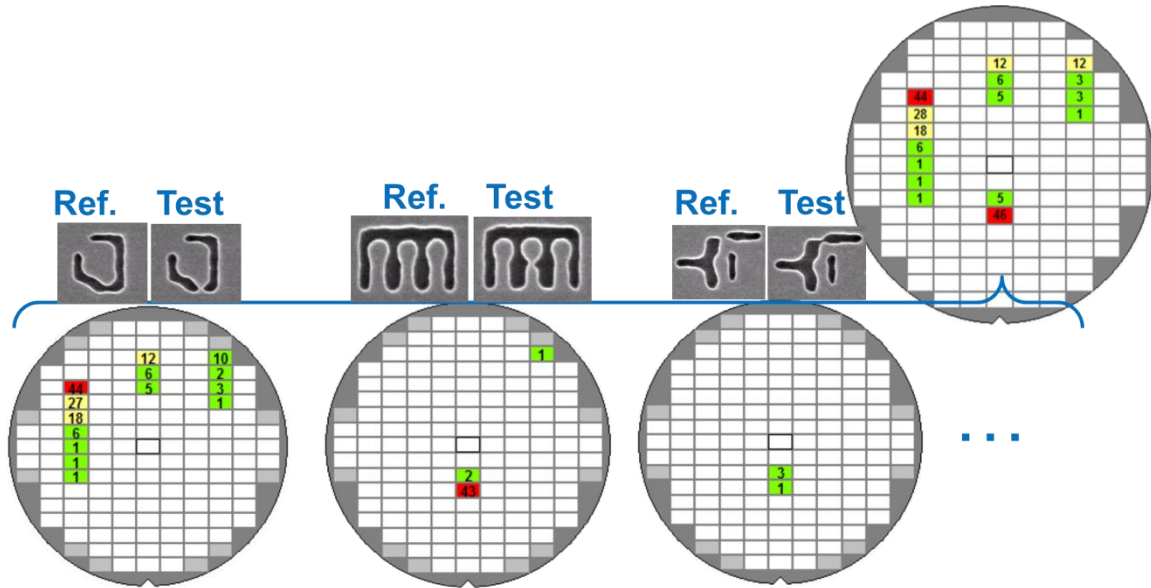


Figure 12. PWD inspection maps showing the different limiting features at positive and negative defocus.

As noted previously, the test mask used in this study contains 200 fm bandwidth OPC features (as shown in Figure 4) that were generated using an extrapolation model based on dose offset without illumination source optimization. To further understand the impact of light source E95 bandwidth on hot spot process window and defectivity, the illumination source must also be considered as design related hotspots detected in ArFi patterning can often be caused by both the illumination source and OPC solutions for the particular features considered. For this study, the Brion TachyonTM product was used to optimize the illumination source for 200 fm E95 bandwidth. The E95 bandwidth condition used was 0.200 pm (200 fm) E95 with a full width half maximum (FWHM) of 0.120 pm. The SMO Tachyon standard optimization flow was used^[10] with the feature layout limited to the hot spots identified as shown in Figure 6. Figure 13 shows the illumination source for the nominal 300 fm condition generated using the full chip layout and nominal 300 fm OPC (left) and for the 200 fm condition generated using the limited hot spot feature list and extrapolated OPC at 200 fm (right).

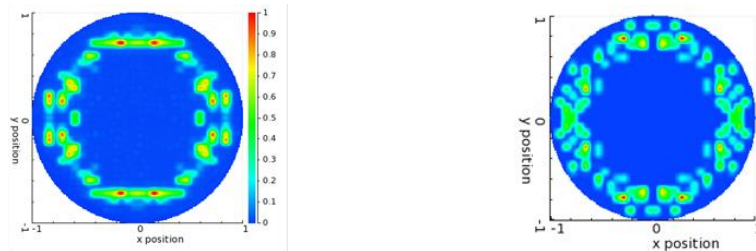


Figure 13. Illumination source generated for the nominal 300 fm illumination source using the full chip layout (left) and for the limited hot spot feature list and 200 fm (right).

The difference in the sources based on the feature sets used in the optimization has a significant impact on the PWD results. The defect mode classification for the PWD wafer with the 200 fm extrapolated OPC, 200 fm limited feature set optimized illumination source, and 200 fm light source bandwidth exposure is shown in Figure 14. The results show a decrease in the process window when compared to the 300 fm nominal results (Figure 11). These results indicate that source optimization using a targeted, limited feature sets by itself is not enough to improve the process window. A complete source mask optimization (SMO) and OPC model generation with proper hot spot weighting are needed to obtain improvement in patterning.

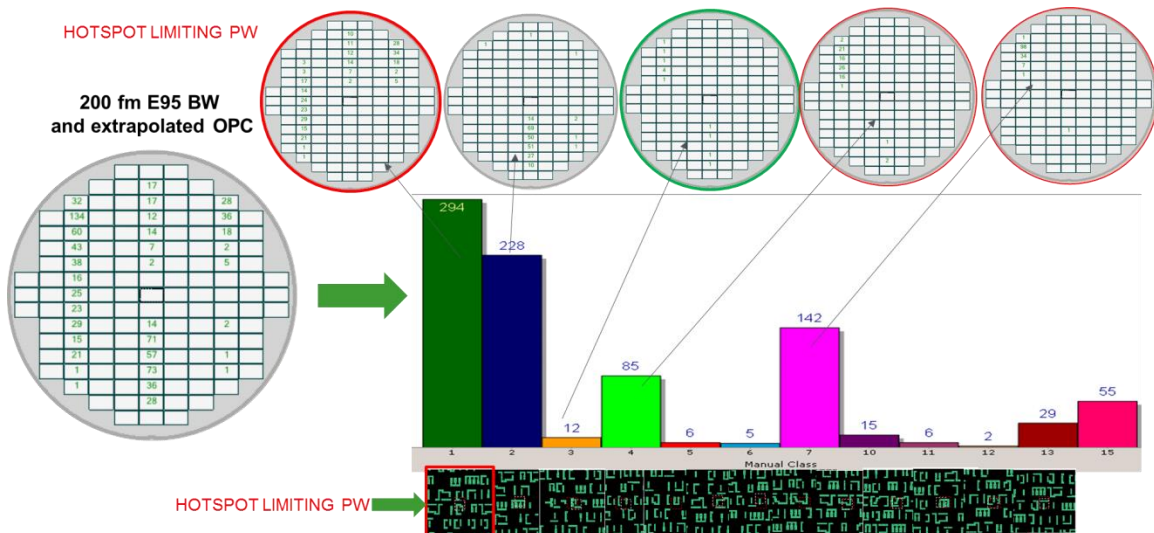


Figure 14. PWD inspection map for the 200 fm bandwidth condition (extrapolated OPC, illumination source, and light source) and classification of key process window limiting hot spot features (right).

To study the impact of varying light source bandwidth on this systematic hot spot performance, PWD analysis on three wafers 1, 2 and 3 with three different laser bandwidth conditions 350, 300, and 200 fm were compared, respectively. The results on the right indicate an incremental improvement for the systematic hot spots with decreasing laser BW in combination with extrapolated OPC. This is in agreement with simulation-based studies that show lower bandwidth improves imaging contrast, thereby reducing the magnitude of hot spots. An overall decrease in defect counts and hot spot types is observed; however, it should be noted that hot spot type 2 shows an increasing trend which needs to be investigated and will require further exposure optimizations.

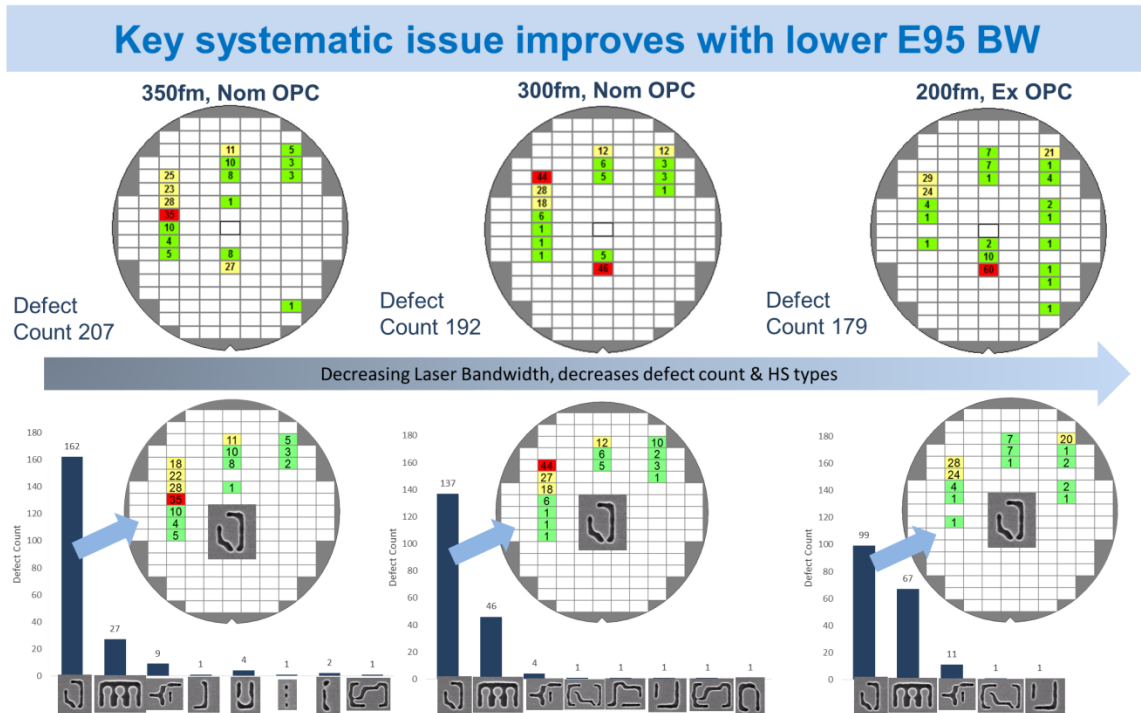


Figure 15. PWD inspection maps for 350 fm (nominal OPC), 300 fm (nominal OPC), and 200 fm (extrapolated OPC).

Fixed offset (Uniformity) wafers

The inspection results shown in Figure 16 are for the 200 fm condition (extrapolated OPC, illumination source, and light source). There is an increase in defect counts as compared to the nominal results shown in Figure 10.

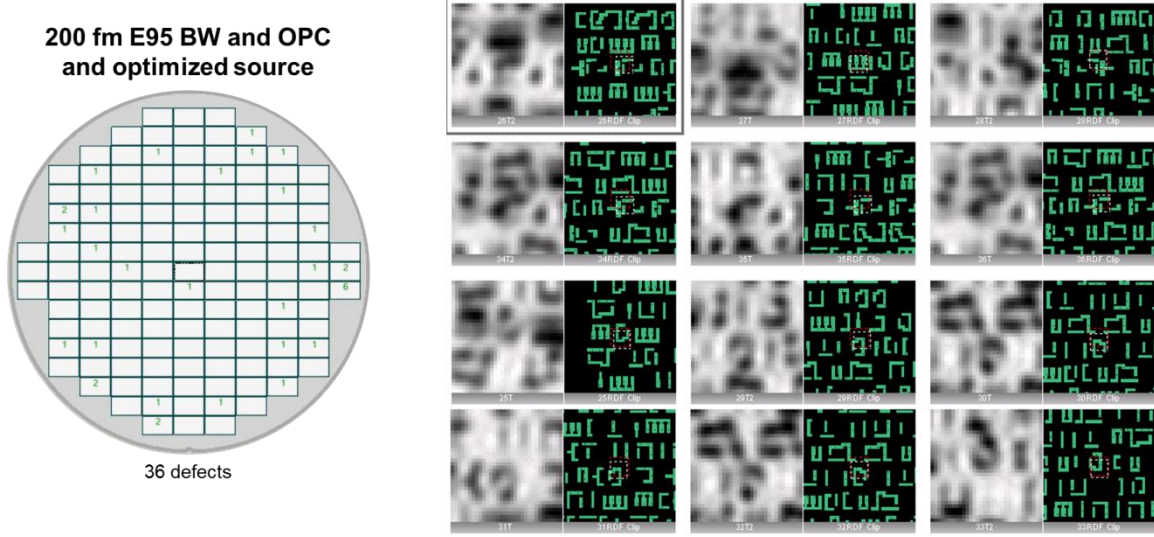


Figure 16. Uniformity wafer inspection map for the 200 fm bandwidth condition (left) and sample detected defects (right). Note that bridging defects are indicated by the dark polarity and broken/pinching defects are indicated by bright polarity.

To further assess the impact of the limited feature set illumination source optimization, the 200 fm condition results can be analyzed by identifying the defect counts for the 200 fm extrapolated and 300 fm nominal OPC mask regions (see Figure 17).

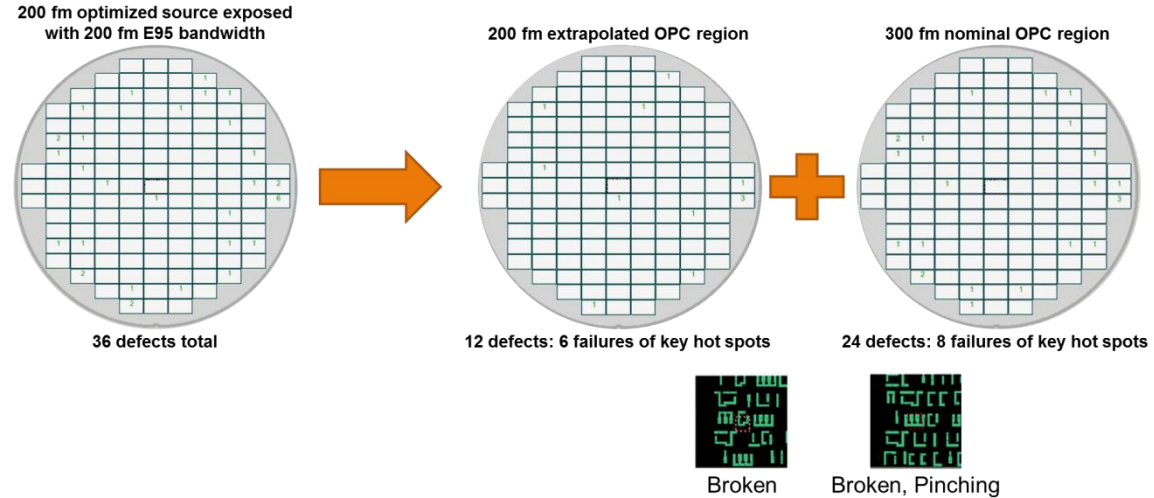


Figure 17. Uniformity wafer inspection map for the 200 fm bandwidth condition divided into the 200 fm extrapolated OPC and 300 fm nominal OPC contributions.

By separating the defects by OPC model, it is observed that lowering the bandwidth of the light source to 200 fm with the extrapolated OPC does improve the defectivity level on the uniformity wafer. However, a

reduction in bandwidth to 200 fm also results in the formation of the key hot spot (HS_05) which is not able to be corrected by the limited feature set illumination source optimization. The fixed offset (Uniformity) inspection maps further demonstrate that source optimization for limited feature sets by itself is not enough and that complete source mask optimization (SMO) and OPC model generation with proper hot spot weighting are needed to obtain improvement in patterning. Similar to the nominal condition results, it should be noted that the defects primarily exist at the edge of the wafer, indicating lower margin due to process and/or topography variations.

CONCLUSIONS

The impact of light source E95 bandwidth on 10 nm Metal 1 Logic features was studied a tunable DUV light source bandwidth technique and the PWD methodology. The PWD findings supplement the traditional analysis methods reported previously^[1-3] and provide more detail on where the process window truly lies as a function of E95 bandwidth. The results demonstrate the effects of E95 bandwidth on non-obvious lithographic features that may limit common process window, and can provide input for the optimal E95 bandwidth that should be used for a process. The significant hot spot dependent responses observed demonstrate the complexities that must be considered when changing imaging conditions (illumination source, OPC model, etc.).

ACKNOWLEDGEMENTS

The authors would like to acknowledge the contributions of xxx for his creation of the 200 fm extrapolated OPC model, yyy for their contributions of aaa, and zzz for bbb.

REFERENCES

- [1] A. Cross et al., Process Window Discovery Methodology Development for Advanced Lithography”, Advanced Semiconductor Manufacturing Conference (2016).
- [2] P. Alagna et al., “Optimum ArFi Laser Bandwidth for 10nm Node Logic Imaging Performance”, Proc. SPIE 9525, Optical Microlithography XXVIII, 952508 (2015).
- [3] P. Alagna et al., “Lower bandwidth and its impact on the patterning performance”, Proc. SPIE 9780, Optical Microlithography XXIX, 978008 (2016).
- [4] P. Alagna et al., “Improving On-Wafer CD Correlation Analysis Using Advanced Diagnostics and Across-Wafer Light-Source Monitoring”, Proc. SPIE 9052, Optical Microlithography XXVII, 905228 (2014).
- [5] U. Iessi et al. “Laser bandwidth effect on overlay budget and imaging for the 45 nm and 32nm technology nodes with immersion lithography”, Proc. SPIE 7973, Optical Microlithography XXIV, 797328.
- [6] N. Seong, et al. “Analysis of the effect of laser bandwidth on imaging of memory patterns”, Proc. SPIE 7140, Lithography Asia 2008, 714042.
- [7] P. De Bisschop et al. “Impact of finite laser bandwidth on the CD of L/S structures“, Journal of Micro / Nanolithography, MEMS and MOEMS (JM3), Vol. 7, No. 3 (2008).
- [8] N. Seong, et al. “Analysis of the effect of laser bandwidth on imaging of memory patterns”, Proc. SPIE 7140, Lithography Asia, 714042 (2008).
- [9] W. Conley et al. “Impact of bandwidth on contrast sensitive structures for low k1 lithography”, Proc. SPIE 9426-6, Optical Microlithography XXVIII, (2015).
- [10] https://staticwww.asml.com/doclib/productandservices/TACHYON_SMO_source_and_mask_co-optimization.pdf

Image contrast enhancement of multiple patterning features through lower light source bandwidth

Paolo Alagna^a, Will Conley^b, Greg Rechtsteiner^b,
Kathleen Nafus^c, Serge Biesemans^c

a) Cymer LLC, Kapeldreef 75, 3001 Leuven, Belgium

b) Cymer LLC, 17075 Thornmint Court, San Diego, CA 92127

c) TEL, resident at imec, Kapeldreef 75, 3001 Leuven, Belgium

ABSTRACT

DUV immersion lithography (ArFi) continues to be the primary lithographic method for semiconductor manufacturers. Use of ArFi lithography requires patterning budget improvements in the range of 1/10 nm especially for interconnect layers^[1]; for advanced process technology nodes, every Angstrom counts. Previous investigations into the effects of light source bandwidth on imaging performance have provided the foundation for this work^[2-10]. This study will focus on the increase in image contrast that 200 fm light source E95 bandwidth enables on Self-Aligned Double Patterning (SADP) and Self-Aligned Quadruple Patterning (SAQP) features. The impact of 200 fm E95 bandwidth on the CD and Edge Placement Error (EPE) performance of core (grating) and block features will be assessed using an imec 7 nm process node test vehicle. The on wafer experimental results will be compared with the simulation predicted responses of the target features to lower light source bandwidth.

1. INTRODUCTION

In the application of low k1 imaging using extreme illumination conditions, DUV-based multiple patterning methods place stringent requirements on light source equipment. Light source key performance indicators include, but are not limited to, the control of energy, wavelength, and bandwidth. Variations in light source Energy control can influence scanner dose control and therefore impact on wafer CD performance. Light source Wavelength directly impacts focus control, with the magnitude varying per scanner model due to differences in lens chromatic aberration. Variations in light source bandwidth impacts imaging contrast (and therefore exposure latitude and CDU) and proximity. Previous studies have determined and quantified the relationships between light source bandwidth performance and on wafer patterning results^[5,6,7].

Light source

Ideally, the light source used for DUV lithography applications should be monochromatic (Figure 2a). This means that the source should output a single wavelength (λ_0) which is fixed and stable over time and space^[4]. In reality due to optical and mechanical limits we know that with the technology currently available that level of performances are not physically achievable.

For a real DUV excimer light source, the effective wavelength oscillates (Figure 2b), losing energy in the region around the target wavelength (λ_0). The final approximation of all the different wavelength components, using a Gaussian or modified Lorentzian^[11] model, leads to a spectrum similar to what has been simplified in Figure 2c.

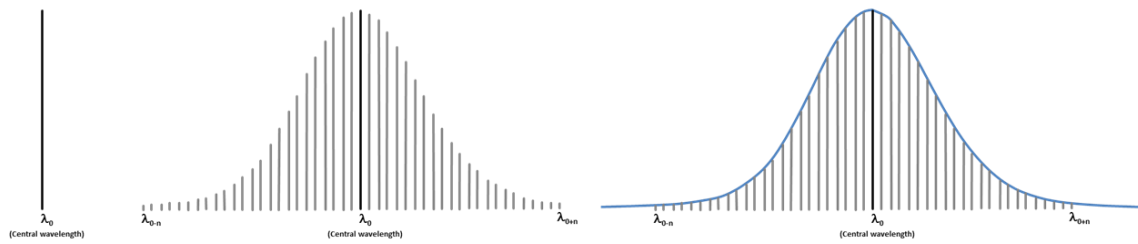


Figure 2. (a) Ideal laser spectrum; (b) Example of real laser spectrum; (c) Example of Gaussian interpolation

In addition to wavelength, another key optical parameter used to characterize an excimer light source for DUV lithography is the bandwidth, which can be represented using two different metrics: Full-Width-Half-Maximum (FWHM) and E95% (Figure 3). FWHM conveys a general representation of the light source spectrum and its changes at half intensity, but it cannot describe the complete spectral shape. The other metric, instead, is based on the 95% integral energy (E95%) of the spectrum, and therefore can be used as a single metric to represent the shape of the spectrum^[12]. In the semiconductor industry, E95% is widely considered the most reliable metric for the ArF light sources used in lithography applications.

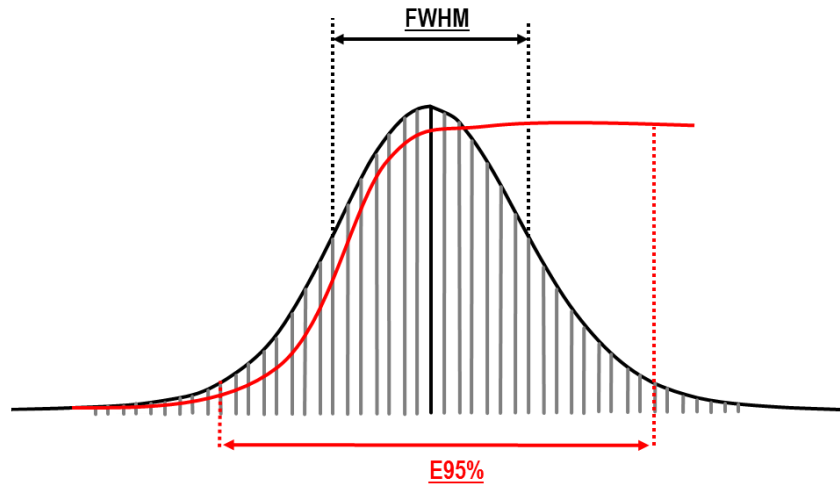


Figure 3. Laser Bandwidth metrics: FWHM and E95%

Projection Lens

Although the research in lens manufacturing area has shown significant progresses in the reduction of aberrations, the technologies presently available do not deliver aberration free optical modules. Among all of the aberration components, chromatic aberration is particularly important for DUV systems because the magnitude of its effect can change as function of wavelength^[13]. This particular parameter emerges because the index of refraction of any optical material changes with wavelength (Figure 3a). As image formation is the result of the superposition of the image intensities of each of the contributing wavelengths, then, due to the chromatic aberration, this superposition leads to a focus blur in the formulated image (Figure 3b).

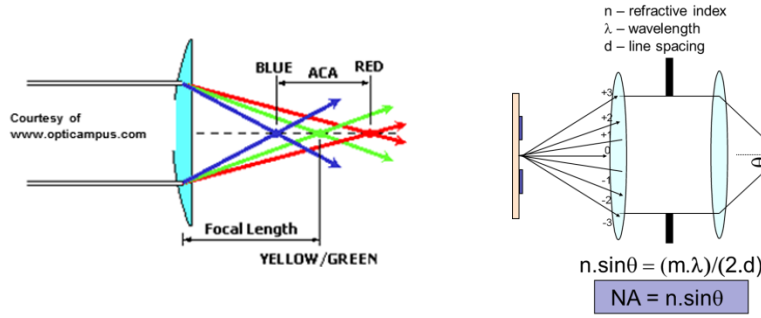


Figure 3. (a) Longitudinal variation of focus, or image position, with wavelength; (b) Pictogram describing of image transfer principle

Therefore, a reduction of the wavelength components (which will be measured as a narrower bandwidth) will lead to a higher image contrast because the blur is reduced.

Image Log Slope

A narrower laser bandwidth will generate a reduction in the image blur, which is also measurable as a better defined energy distribution at wafer level, affecting primarily the slope of the aerial image intensity (Figure 4a).

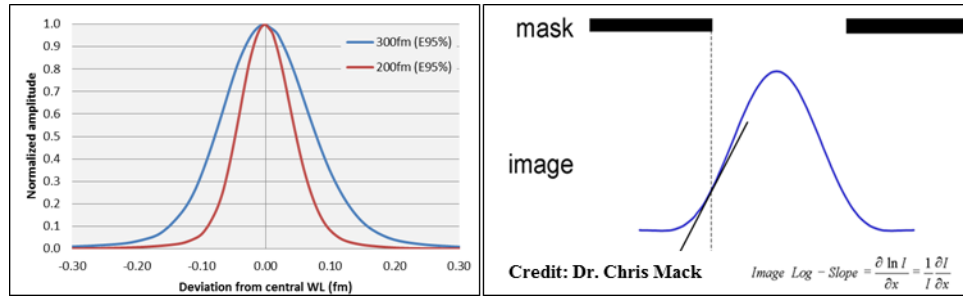


Figure 4. (a) Pictogram of bandwidth reduction; (b) ILS description

The slope of the image intensity as of function of position (dI/dx) measures the steepness of the image in the transition from bright to dark. However, to be useful it must be properly normalized. For example, doubling the intensity of the light will double the slope, but the image quality will not be improved. Dividing the slope by the intensity will normalize out this effect. The resulting metric is called the image log-slope (Figure 4b)^[14,15]:

$$Image\ Log - Slope = \frac{1}{I} \frac{dI}{dx} = \frac{d \ln(I)}{dx} \quad [1]$$

Equation [1] describes the log-slope measured at the nominal (desired) line edge. Since variations in the photoresist edge positions (linewidths) are typically expressed as a percentage of the nominal linewidth, the position coordinate x can also be normalized by multiplying the log-slope by the nominal linewidth w , to

give the normalized image log-slope (NILS).

$$NILS = w \frac{d \ln(I)}{dx} \quad [2]$$

Exposure Latitude (EL)

Exposure latitude (EL) is defined as the range of exposure, as a percentage of the nominal exposure dose, which keeps the resulting feature width within a target range of the nominal size ^[14,15].

$$w \frac{\partial \ln E}{\partial CD} = \frac{1}{2} NILS \quad [3]$$

Equation [3] describes how, in an ideal regime (perfect photoresist with infinite contrast), EL is expressed as the slope of a critical dimension (CD) versus exposure dose (E) curve, $\partial CD / \partial E$, where w is the nominal feature width and NILS, are related.

An increase in contrast (and therefore also NILS) would reduce the dose sensitivity $\partial CD / \partial E$, increasing the exposure latitude (EL). As equation [3] considers the case of an ideal photoresist it does not take into account the contributions coming from the photo reactive materials ^[14,15]. Including those additional variables and applying the proper simplification the formula could be re-written as follows:

$$\% \text{ Exposure Latitude} \approx \alpha (NILS - \beta) \quad [4]$$

where β can be interpreted as the minimum NILS required for an acceptable image in photoresist to appear and α is the added exposure latitude for each unit increase in NILS above the lower limit β .

Local Critical Dimension Uniformity (LCDU)

LCDU can be defined as the critical dimension variation within the exposed field. As an exposure field is the direct replication of the image transferred from the mask to the wafer through the projection lens, it can be determined how the LCDU encompasses the mask and optical components of the system. When discussing masks (often called also reticles), it must be considered that the features imprinted on the quartz substrate contain an intrinsic CD error which is not linearly transferred through the projection lens to the wafer. In other words, CDU of the mask is not equal to the LCDU on the wafer.

This specific error called Mask Enhancement Error Factor (MEEF) is described as ^[16,17,18]:

$$MEEF = \frac{\Delta CD_{wafer}}{\Delta CD_{reticle} \times R_{lens}} \quad [5]$$

where R_{lens} is the magnification rate of the projection lens.

The ideal MEEF value is equal to 1, which means that the errors present in the mask are directly transferred into the wafers and measured in the local field. In practice, the resist, feature size and pitch, process conditions such as exposure energy and focus errors, illumination conditions, and lens aberrations influence the MEEF. Therefore, due to optical and process factors the Mask Error Enhancement Factor is always greater than 1.

Developing and combining ^[16,17,18] equations [3] and [5], can obtain (after the proper simplification) in an elementary form the correlation between MEEF and EL is obtained:

$$MEEF \sim \frac{1}{(pitch \times EL)} \quad [6]$$

Therefore, a higher aerial image contrast (which is driving up the EL) yields a smaller MEEF.

In summary, an increase of the aerial image (NILS) through the reduction of light source bandwidth results in an increase of the exposure latitude (EL) and a reduction of the LCDU (due to a decrease in MEEF).

2. EXPERIMENTAL PLAN

The target of this work was to assess the impact of laser driven contrast enhancement on two different DUV patterning solutions:

- Self-Aligned Double Patterning (SADP)+ Blocks
- Self-Aligned Quadruple Patterning (SAQP) + LE³ Blocks

The activities were conducted in imec facilities in Leuven (Belgium) using the following tools:

Tool	Model	Notes
Track	CLEAN TRACK™ LITHIUS Pro™ Zi [TEL]	
Exposure tool	NXT:1970Ci [ASML]	FlexRay / Flexwave
Light source	XLR:760 [Cymer]	Nominal E95% = 300 fm ± 5 fm Low E95% = 200 fm ± 5 fm

The starting conditions for the two solutions stated above are both with the mask and illuminaton source having been optimized (SMO) at 300 fm light source bandwidth.

Source

A reduction of light source E95% requires a correction of the illumination condition to re-optimize the energy distribution in order to maintain optimal contrast at wafer level, as illustrated in Figure 5.

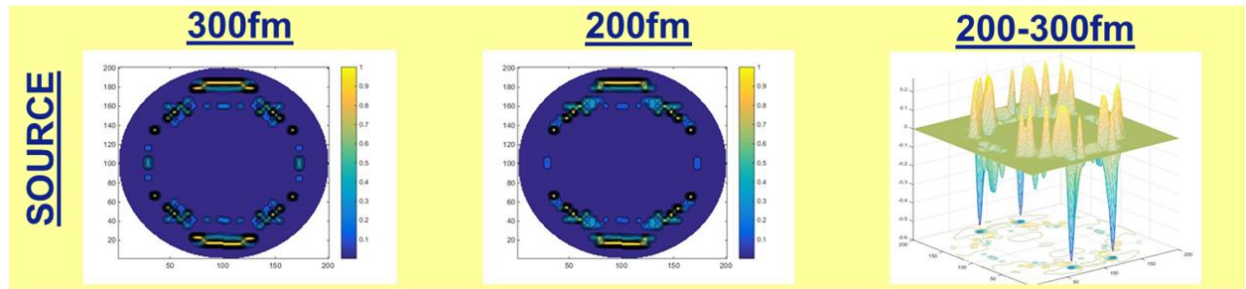


Figure 5. Examples of changes in the a source optimized at 300 fm and 200 fm of E95%

OPC

The models used to apply the optimal Optical Proximity Corrections (OPC) should comprehend the light source bandwidth, therefore a change in bandwidth results in changes in the model solution as shown in Figure 6.

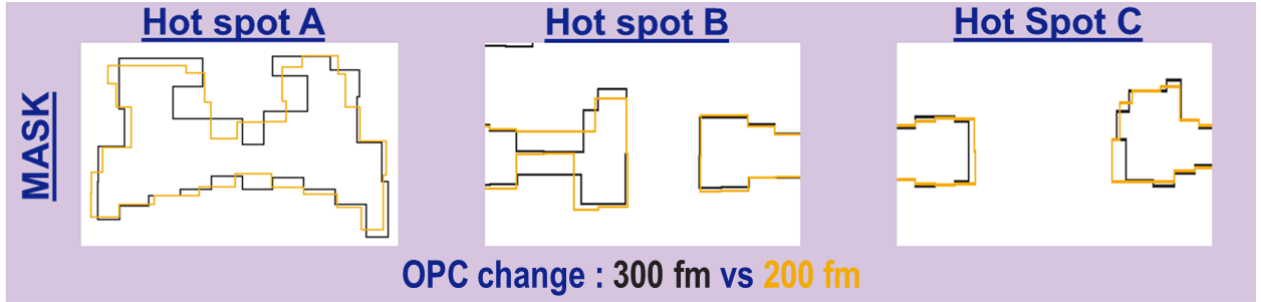


Figure 6. Examples of changes OPC comparing 300 fm and 200 fm of E95%

Use of reduced bandwidth should be combined with full Source Mask Optimization (SMO). For masks that have already been created, the full SMO cannot be modified; however, the source by itself can be optimized (SO) for the existing features. In this study, the data has been collected at the nominal 300 fm bandwidth condition and at the semi-optimized region (SO only) using 200 fm bandwidth. Source optimization was performed using Tachyon platform from BRION. Standard optimization flow was used^[19] considering TE polarization (DoP of 0.97), 6% attenuated PSM mask with M3D (3D mask calculation) model and also an NTD resist model. .

3. Self-Aligned Double Patterning + Blocks (PTD)

The first application tested was the patterning of the PTD Blocks on the SADP flow described Figure 8.

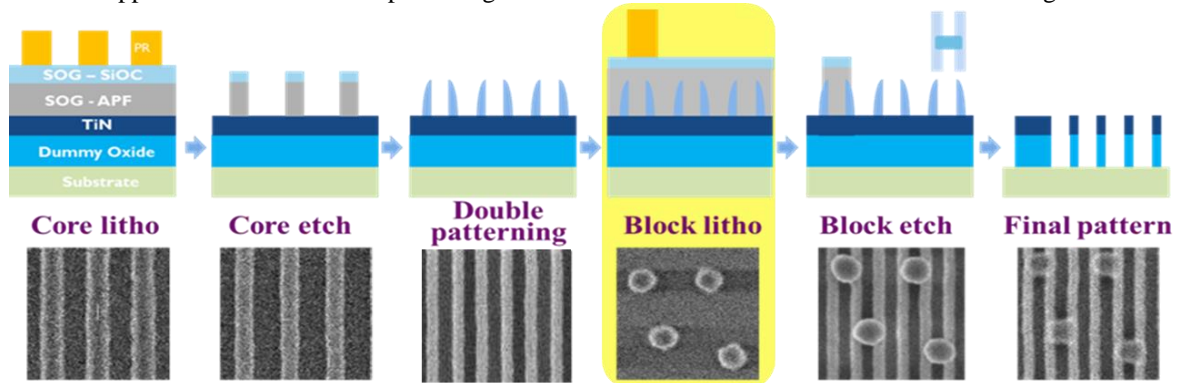


Figure 8. SADP+Blocks flow used on our experiment

The Blocks features which were considered in this experiment are characterized by a matrix of round pillars with a target CD on wafer of 51 nm. From a design prospective, the matrix is generated by repeating the same four-OPC-fingerprint multiple times (Table 1a).

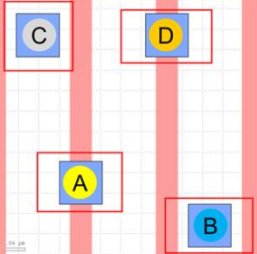
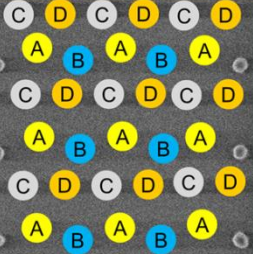
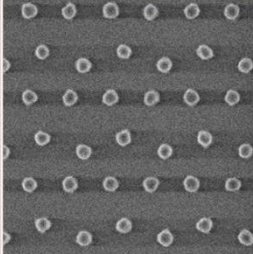
Reference mask feature	Original Source	200fm (SO) Source Optim.
		
Pitch (nm) A-B = 126 A-C = 132 A-D = 150 B-C = 233 B-D = 166 C-D = 132	4 OPC groups	Target ADI CD (nm) = 41 ± 3

Table 1. (a) Litho pattern; (b) OPC group distribution; (c) OPC details

The analysis of the patterning results was conducted by grouping the OPC by design characteristics (A, B, C, D) analyzing them individually.

The source and optimization comprehended a wide selection of the Block matrix GDS (Table 2a), and showed how the reduction of the laser bandwidth effected the energy distribution at pupil level (Table 2b and 2c).

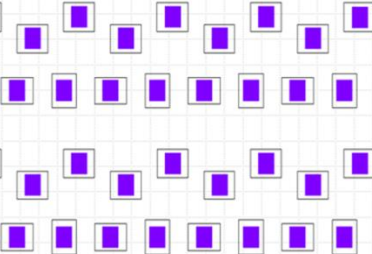
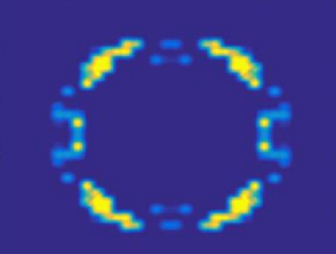
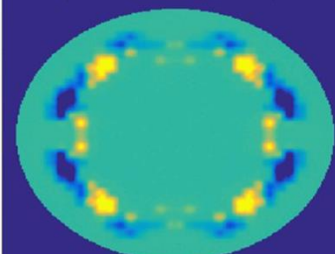
Reference mask feature	300 fm (Nominal)	Changes at 200 fm SO
		

Table 2. (a) Litho pattern; (b) OPC group distribution; (c) OPC details

The process window analysis was conducted on full stacked wafers, exposing focus exposure matrixes (FEM) with 0.5 mJ/cm^2 steps in dose and 10 nm steps in focus. The measurement was performed using Hitachi CD-SEM CG6300, collecting 54 block measurements per exposure field (27 features measured in 2 intra-field positions). The settings used for the metrology are reported in Table 3.

SADP Blocks	ADI Inspection
Accelerating_voltage	500 V
Probe_current	8.0 pA
Magnification	160K
Digital_Zoom	1
Number_of_frames	8
Field_Size (um)	0.819 x 0.819
Pixel	1024 x 1025
Filter	None

Table 3. Block CD-SEM metrology settings

Both theory and previous experimental activities^[5,7,8], indicate that narrowing down only the light source bandwidth, (without performing any other action) is possible to estimate an increment of EL with limited depth of focus degradation. In this study, however, it has been demonstrated that working in a semi-optimized-regime (low bandwidth and source optimized) it is possible to maintain the optimal response in terms of EL increase compensating for any loss in DOF, or in cases like the ADI Blocks shown in Figure 11 even increase the original margin.

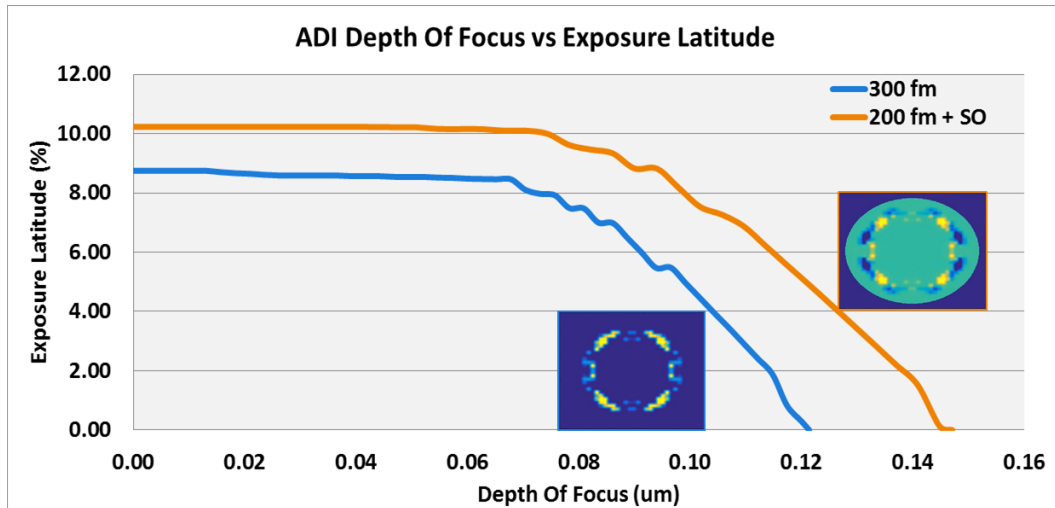


Figure 11. Exposure latitude vs Depth of Focus plot : +20% DOF (+30 nm) and +11% EL (+1 %)

The second area of investigation involved the assessment of local CDU in the same semi-optimized-regime. Based on the Bossung plot data already available was possible to extract a dose offset of +1 mJ/cm² to be applied at the low bandwidth exposure to match the same nominal target CD. The metrology sampling plan for this study can be summarized as follows: 229 exposure fields x 12 points per field x 27 pillar per measurement point > 74K measurements per wafer.

The measurements were sorted by OPC type and analyzed separately. The summary as reported in figure 13, shows that there is a dependency between the OPC structure and the CD uniformity response. If an average among all the features is considered, the 3 sigma reduction is on the order of 0.1 nm or 7%.

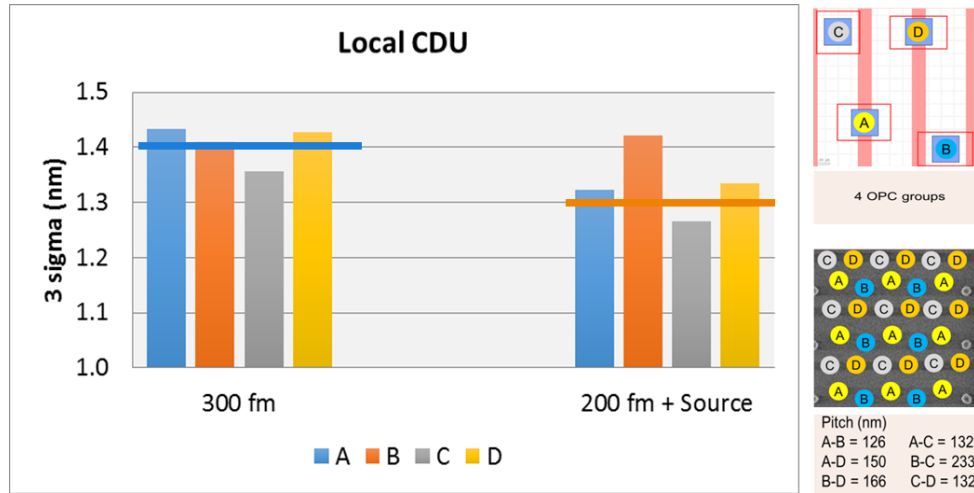


Figure 13. (a) Litho pattern; (b) OPC group distribution; (c) OPC details

Leveraging the capability offered by Hitachi CD-SEM to provide the measurement of the pillars positions based on the image center of gravity, the error in misplacement among the pillars can be computed. The block positions in this process are extremely important in order to have the proper alignment on the core features underneath. The results show an incremental (but statistically significant) improvement in the positioning of the blocks (figure 14)

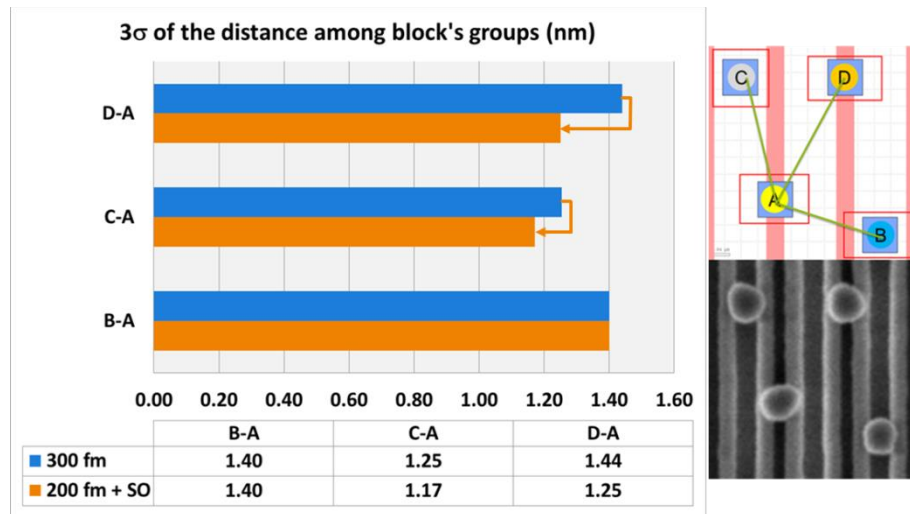


Figure 14. (a) Litho pattern; (b) OPC group distribution; (c) OPC details

4. APPLICATION ON SAQP + LE³ BLOCKS

The second application tested was the patterning of the NTD blocks on the SAQP flow described in figure 15.

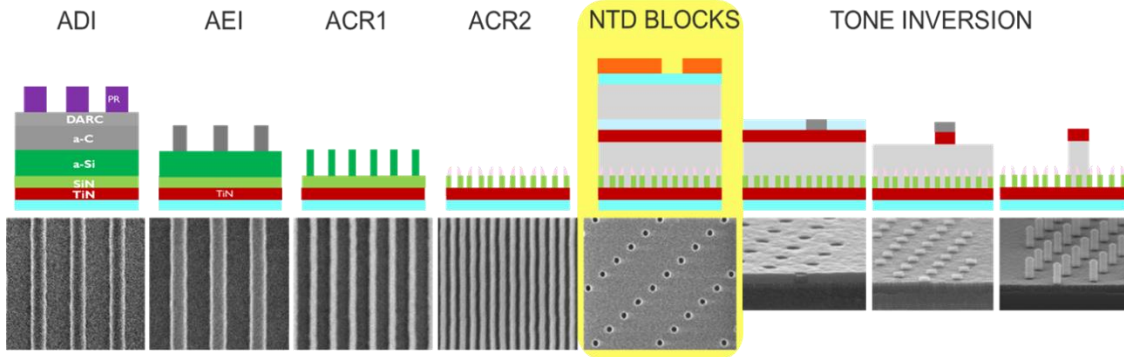


Figure 15. SAQP+Blocks flow used on our experiment

Despite the official patterning flow involve triple litho-etch (LE³) steps for the blocks, we have performed in this phase the analysis only after the first etch. Litho results previously measured (in another area of the matrix) were then used to adjust the best exposure conditions in order to achieve the optimal AEI targets, as shown in the table 4.

Reference mask feature	After Litho	After Etch
Blocks LE Distance (nm) X = 405 Y = 94	ADI Target (nm) X = 41 ± 3 Y = 52 ± 3	ADI Target (nm) X = 21 ± 3 Y = 32 ± 3
Blocks LE ³ Distance(nm) X = 135 Y = 64		

Table 4. SAQP Blocks ADI and AEI targets

We have applied then the same analysis approach used previously, proceeding in tree steps: Source optimization, process window analysis and investigation on CD Uniformity changes

Source Optimization and 200 fm (E95%)

Table 5 is showing the energy distribution changes after the optimization at 200 fm (E95%). The scale indicates the normalized pixel energy intensity, and it is possible to estimate a variation in the distribution of $\pm 10\%$

Reference mask feature	300 fm (Nominal)	Changes at 200 fm SO

Table 5. LE Block Source Optimization

Process Window analysis

From the previous table 4, is possible to see how, unlike the SADP Blocks, the shape for our target features is more elliptical and therefore we must consider two separate CD targets: one for the X direction and the other for the Y direction. For this reason we have decided to analyze the common process window which basically indicates the ranges of doses and focuses defining the Blocks within their specifications.

Note concerning the metrology

Also for this second part of the experiment the Hitachi CG6300 CD-SEM was used, and in our particular case the settings reported in Table 6 were utilized.

LE Blocks	AEI Inspection
Accelerating_voltage	800 V
Probe_current	8.0 pA
Magnification	150K
Digital_Zoom	1
Number_of_frames	32
Field_Size	0.902 um, 0.902 um
Pixel	512 x 512
Filter	None

Table 6. AEI Block CD-SEM metrology settings

It must be said that the ellipsoidal shapes of the blocks offer a metrology challenge. The electron beam scanning direction is fixed therefore even if the CD-SEM extrapolate a fitting out of the signal measured, the measurement in the Y direction will be much more noisy compared to the one in X direction. To minimize this effect we have repeated the measurement two times. The first one, using the standard image orientation, was used to extract the measurement of X direction, while the in the second measurement the target feature was rotated by 90 degrees, extracting the Y direction measurement (Figure 15).

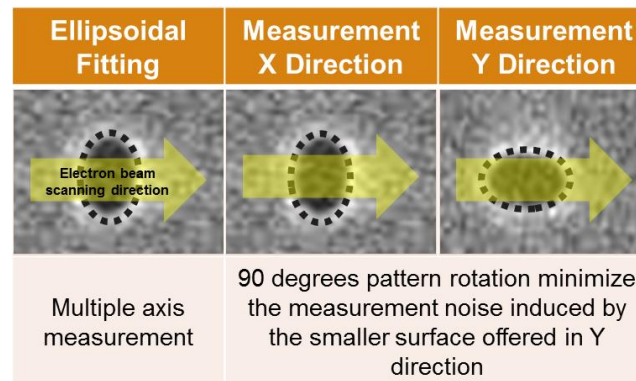


Figure 15. AEI Block CD-SEM metrology settings

Process window analysis was performed exposing the usual focus exposure matrix, measuring then 20 blocks per exposure field on each direction (2 intra-field locations, 10 blocks for each location, measuring horizontal and vertical orientations)

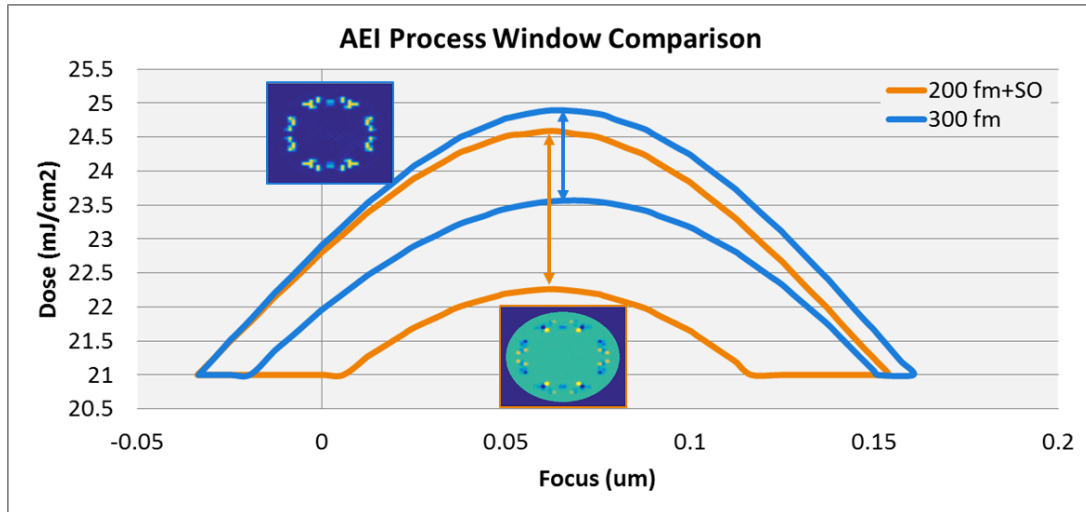


Figure 16. LE Block Process Window comparisons

The process window analysis (Figure 16) shows an increment of net exposure latitude (EL) by 4% without any significant reduction in terms of depth of focus (DOF). It is however interesting to notice how neither for the SADP Blocks (PTD process) nor on the SAQP Blocks (NTD process) a shift in focus was measured in the samples exposed at 200 fm (E95%)

Analysis of the uniformity of the critical features

Due to limitations provided by the test mask used, it was not possible to assess the local CD uniformity. Our target features, in fact, were only located in a 3000x500 μm area in the reticle used. However, we have noticed that another potential indicator which could help us to have information on the contrast-driven changes could have been what we have called field of view CD uniformity (FOV CDU). The field of view we are referring to is the CD-SEM one. As shown in figure 17, what can happen is that within the metrology capturing area the shape of the blocks can differs from the target.

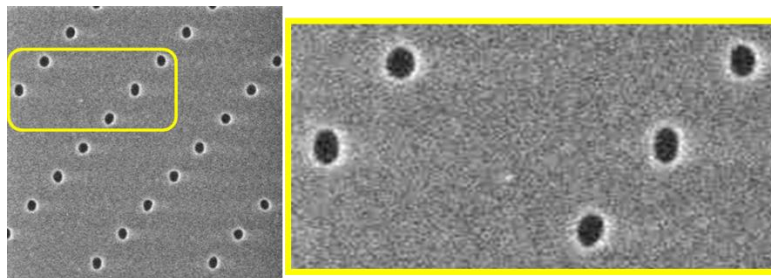


Figure 17. FOV concept. Block deformation within the same CD-SEM field of view

The extended analysis performed over more than 17K blocks measured both in nominal and contrast enhancement conditions, showed how the reduction of bandwidth in a semi-optimize regime contributes to a statistically meaningful CDU improvement. In our specific case it was possible to assess a net reduction of the 3σ of 0.2 nm in figure 18.

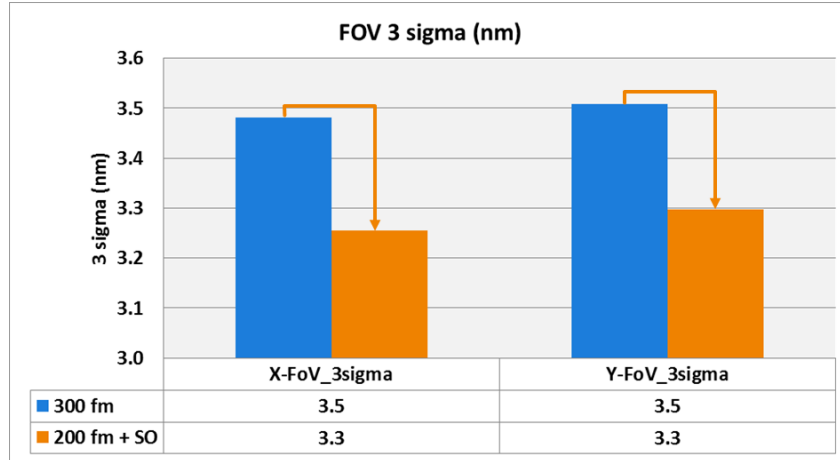


Figure 18. FOV CD Uniformity

5. CONCLUSION

Bandwidth driven image contrast enhancement has been verified on wafer for SADP and SAQP process flows, concluding that in a semi-optimized regime (source optimization only), lower bandwidth delivered significant margin improvements for PW and LCDU. However to maximize the potential benefit coming from the laser-induced image contrast enhancement, full source and mask optimization (SMO) should be performed. Further studies will include simulation and experimental activities in a 200 fm fully optimized (SMO) regime.

6. ACKNOWLEDGEMENTS

The authors would like to acknowledge Marc Demand and Soichiro Okada of Tokyo Electron at imec for their contribution to the processing of this experiment. We would also like to thank imec for their enablement of collaborative projects such as this one and finally Mircea Dusa of ASML for his thoughtful insights and discussion.

REFERENCES

- [1] 2015 International Technology Roadmap for Semiconductors (ITRS); http://www.semiconductors.org/main/2015_international_technology_roadmap_for_semiconductors_its/
- [2] Umberto Iessi et al. "Laser bandwidth effect on overlay budget and imaging for the 45 nm and 32nm technology nodes with immersion lithography." Proc. SPIE 7640, Optical Microlithography XXIII, 76402B (March 03, 2010); doi:10.1117/12.846552.
- [3] Nakgeun Seong et al., "Analysis of the effect of laser bandwidth on imaging of memory patterns." Proc. SPIE 7140, Lithography Asia 2008, 714042 (December 04, 2008); doi:10.1117/12.804557.
- [4] De Bisschop P et al., "Impact of finite laser bandwidth on the critical dimension of l/s structures." J. Micro/Nanolith. MEMS MOEMS. 0001;7(3):033001-033001-16.
- [5] Will Conley et al., "Impact of bandwidth on contrast sensitive structures for low k1 lithography." Proc. SPIE 9426, Optical Microlithography XXVIII, 942607 (March 18, 2015); doi:10.1117/12.2085826.
- [6] R. C. Peng et al., "Effects of laser bandwidth on iso-dense bias and line end shortening at sub-micron process nodes." Proc. SPIE 6520, Optical Microlithography XX, 65203S (March 27, 2007); doi:10.1117/12.713080.
- [7] Paolo Alagna et al., "Optimum ArFi laser bandwidth for 10nm node logic imaging performance." Proc. SPIE 9426, Optical Microlithography XXVIII, 942609 (March 18, 2015); doi:10.1117/12.2085823.
- [8] Paolo Alagna et al., "Lower BW and its impact on the patterning performance." Proc. SPIE 9780, Optical Microlithography XXIX, 978008 (March 16, 2016); doi:10.1117/12.2219945.
- [9] Armen Kroyan et al. "Modeling the effects of excimer laser bandwidths on lithographic performance." Proc. SPIE 4000, Optical Microlithography XIII, 658 (July 5, 2000); doi:10.1117/12.389057.
- [10] Brunner T et al., "Laser bandwidth and other sources of focus blur in lithography." J. Micro/Nanolith. MEMS MOEMS. 0001;5(4):043003-043003-7.
- [11] Ivan Lalovic et al., "Fast and accurate laser bandwidth modeling of optical proximity effects." Proc. SPIE 6730, Photomask Technology 2007, 67301X (October 30, 2007); doi:10.1117/12.746594.
- [12] Armen Kroyan et al., "Effects of 95% integral vs. FWHM bandwidth specifications on lithographic imaging." Proc. SPIE 4346, Optical Microlithography XIV, 1244 (September 14, 2001); doi:10.1117/12.435661.
- [13] Lai K et al., "Understanding chromatic aberration impacts on lithographic imaging." J. Micro/Nanolith. MEMS MOEMS. 0001;2(2):105-111.
- [14] Chris Mack, "Using the Normalized Image Log-Slope part 1 &2" The lithography expert Winter and Spring 2001
- [15] Michel Klaassen et al. "Dynamic performance of DUV step-and-scan systems and process latitude." Proc. SPIE 4000, Optical Microlithography XIII, 776 (July 5, 2000); doi:10.1117/12.389070.
- [16] Richard Schenker et al., "The MEEF NILS divergence for low k1 lithography." Proc. SPIE 6730, Photomask Technology 2007, 67301M (October 30, 2007); doi:10.1117/12.742273.
- [17] Marina V. Plat et al., "Impact of optical enhancement techniques on the mask error enhancement function (MEEF)." Proc. SPIE 4000, Optical Microlithography XIII, 206 (July 5, 2000); doi:10.1117/12.389009.
- [18] Jan B. van Schoot et al., "Mask error factor: causes and implications for process latitude." Proc. SPIE 3679, Optical Microlithography XII, 250 (July 26, 1999); doi:10.1117/12.354338.
- [19] https://staticwww.asml.com/doclib/productandservices/TACHYON_SMO_source_and_mask_cooptimization.pdf

Advances in DUV Light Source Sustainability

Yzzer Roman, Dinesh Kanawade, Walt Gillespie, Siqi Luo, Mark Thever, Thomas Duffey, Kevin O'Brien, Rahul Ahlawat, Andrei Dorobantu, Eric Gross, and Eric Mason,
Cymer LLC (an ASML Company),
17075 Thornmint Ct., San Diego, CA, 92127, USA

ABSTRACT

Cymer continues to address several areas of sustainability within the semiconductor industry by reducing or eliminating consumption of power and specific types of gas (i.e. neon, helium) required by DUV light sources in order to function. Additionally, Cymer introduced a new recycling technology to reduce the dependence on production of raw gases. In this paper, those initiatives that reduce the operational cost, environmental footprint, and business continuity risk will be discussed.

Cymer has increased the efficiency of its light sources through improvements that have resulted in energy output increase while maintaining the same or requiring less power consumption. For both KrF and ArF systems, there have been component [1], system, and architecture improvements [2] that allowed customers to increase energy efficiency and productivity. An example of module improvements is the latest MO chamber that helped reduce power consumption by ~15%. Future improvements aim to continue reducing the power consumption and cost of operation of the install base and new systems.

The neon supply crisis in 2015 triggered an intensive effort by the lithography light source suppliers to find ways to minimize the use of neon, a main consumable of the light source used in DUV photolithography. Cymer delivered a multi-part support program to reduce natural resource usage, decrease overall cost of operation, and ensure that chipmaker's business continuity risk is minimized. The methods used to minimize the use of neon for 248 nm and 193 nm photolithography that offered significant relief from supply constraints and reduction of business continuity risk for chipmakers were described in previous work [3]. In this paper, results from the program will be presented.

In addition, techniques to capture the neon effluent and re-purify it within the semiconductor fabs have been pursued. For example, Cymer has developed and validated a neon recycling system for ArF light sources that resides within the chipmaker's fab. Cymer has partnered with a global gas supplier to develop a system capable of capturing, recycling and delivering >90% of the total neon gas required by multiple ArF light sources through automated operation, including online analysis. In this paper, the neon recycle system performance as demonstrated by a quantitative analysis of facility-supplied gas versus the recycled neon in ArF light source performance will be discussed.

Similarly, DUV light sources have historically used helium as a purge gas in the critical line narrowing module (LNM) to achieve stable wavelength and bandwidth control. Helium has a low coefficient of index of refraction change vs. temperature relative to nitrogen and provides efficient cooling and purging of critical optics in the LNM. Previous work demonstrated how helium consumption can be reduced and still achieve stable performance under all operating conditions [1]. In this paper, results of eliminating the use of helium will be described.

Keywords: DUV, ArF, KrF, sustainability, neon, helium, nitrogen, GLX, neon recycle, neon reduction

1. INTRODUCTION

A constant push to conserve energy and reduce usage of natural resources is primarily driven by the goal of sustainable semiconductor manufacturing and from the need to reduce the cost of integrated circuit photolithography. This push has resulted in semiconductor equipment manufacturers reducing their respective environmental footprints. Cymer has the industry's largest light source installed base (approximately 2,500 systems operating across 150+ facilities worldwide) and Cymer's sustainability program has had a direct and significant impact on the worldwide efforts to reduce the environmental footprint of the semiconductor industry [4].

Cymer has reduced the cost of operating its light sources through a sustainability program that focuses on reducing or eliminating the major components of its operating cost: energy, helium, and neon. Additionally, this reduction was aimed at relieving pressure from rising energy and consumable costs.

Cymer's single chamber (ELS) light sources have been used for DUV lithography in the semiconductor industry for approximately three decades [5]. Similarly, dual chamber (XL) light sources were first introduced for argon-fluoride (193 nm) lithography over a decade ago [6]. Both single and dual chamber platforms have a history of continuous improvements in power efficiency [2, 7] and cost reduction over time [1, 3].

At time of publication, neon and other rare gases have already stabilized in supply continuity and prices, in part from the demand reduction that resulted from Cymer's efforts [3]. However, this market remains fragile and subject to volatility from supply disruptions. Cymer aims to further counter this instability and mitigate business continuity concerns with the newly introduced neon recycle system.

2. POWER EFFICIENCY IMPROVEMENT

Cymer has improved the energy efficiency ratio since the first generation of ArF light sources (XL) with its dual chamber (MOPA) technology (see Figure 1). Initially, the improvements were done by increasing the repetition rate at which the light sources operate since the power output is directly proportional to the repetition rate. Repetition rate increase required changes to the pulsed power design to account for tighter timing requirements [8].

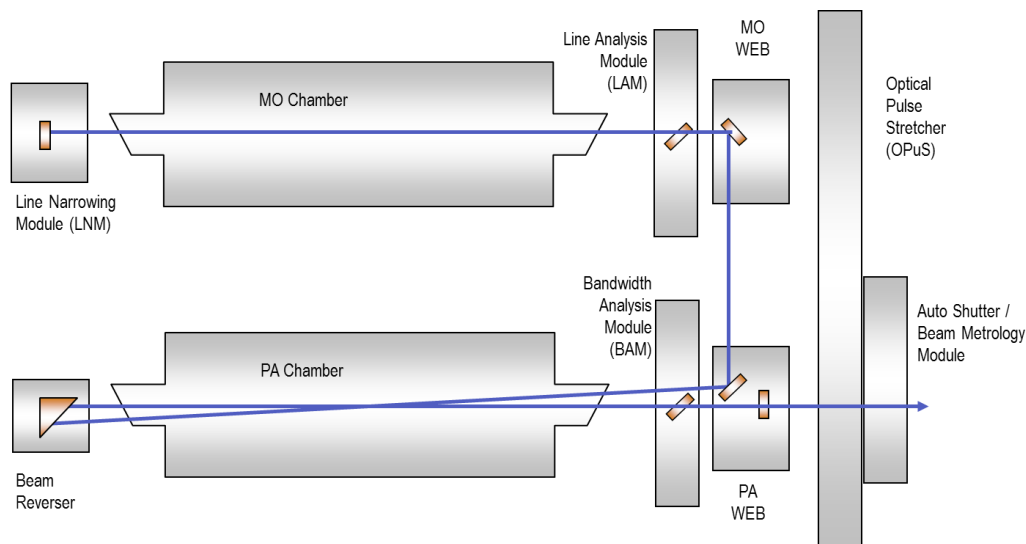


Figure 1. MOPA system architecture and optical path

A significant improvement in the overall system efficiency was achieved by the introduction of the recirculating ring technology (XLR) that allowed higher power output without increasing the repetition rate or input power (see Figure 2) [9]. This technology allowed higher pulse energy output and helped extend module lifetime [2].

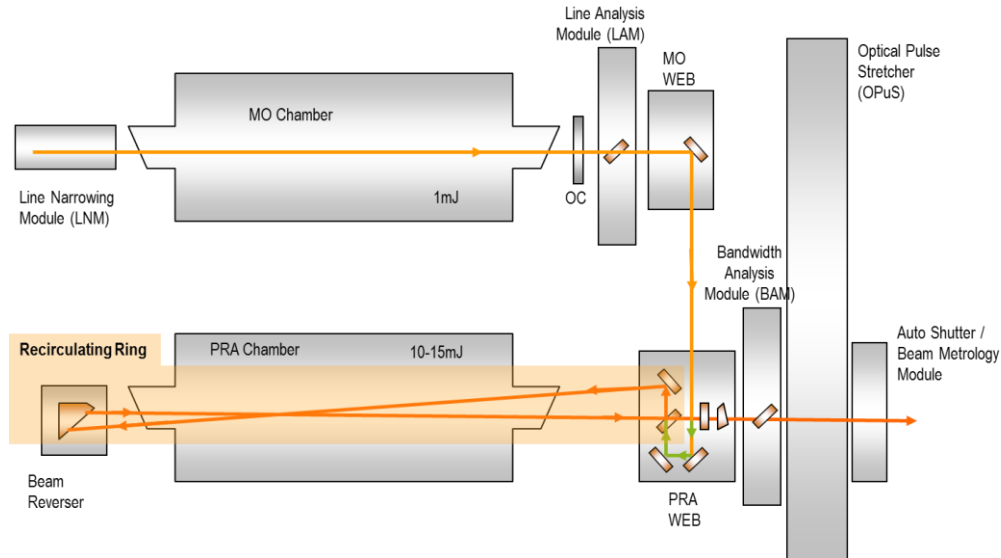


Figure 2. Optical path in XLR systems with recirculating ring technology

As the lithography manufacturing requirements cease to focus on power output for productivity, additional increase in efficiency begins to center on internal efficiency of sub-systems and individual modules. The major contributor to power consumption in Cymer's XL platform is the pulse power sub-system that includes the Solid State Pulse Power Module (SSPPM), Master Oscillator (MO), and Power Ring Amplifier (PRA) chambers. The latest design improvements to the MO chamber contribute to efficiency increase by reducing power consumption by ~15% [1]. This MO chamber technology has had a direct impact in reducing the power consumption across the XLR installed base as well as the leading edge XLR 700ix.

Future improvements will continue to increase efficiency by reducing power consumption in the long term. Improvements to module and sub-system efficiency will be complemented by studying the light source operation and determining idle modes and production readiness (see Figure 3).

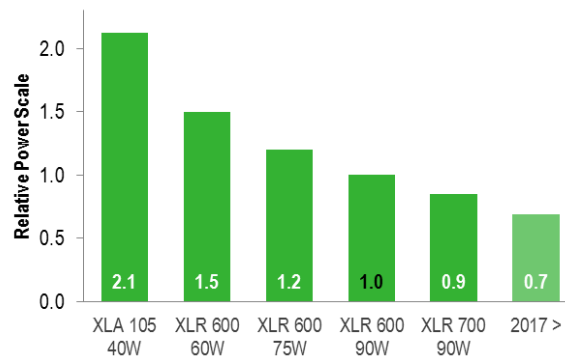


Figure 3. Relative power scale across light source models and power configurations

3. HELIUM REDUCTION AND ELIMINATION

Helium, a non-renewable resource, is primarily produced as a by-product of natural gas extraction. There are only a few sources of helium that produce the majority of the world's supply: Qatar, USA, Russia, and more recently Tanzania.

The limited availability and sourcing factors create a fragile supply of this rare gas, for which there was a recent major shortage [10, 11]. This shortage led to the search for a reduction and an eventual elimination of helium as a consumable.

The Line Narrowing Module (LNM) is responsible for the wavelength and bandwidth control of the light source; the module currently uses helium to displace air from its internal optical components. Helium's specific heat and thermal conductivity, UV transparency, and inert properties make it the ideal purge gas for excimer light source optics. Additionally, its index of refraction does not significantly change as the temperature changes, which minimize beam disturbances when the light source is firing.

Cymer implemented a helium reduction program, which cut the annual consumption and therefore the cost by 50% without impact to wavelength or bandwidth performance [1] across the installed base. To completely replace helium as the purge gas, nitrogen was used in stressful test conditions that increased the operating duty cycle from 30% (LDC) to 75% (HDC) within a short period of time; typical HVM operating duty cycles generally remain below 40%. Test results using nitrogen in a helium-compatible LNM show that some light source specifications are not met under certain operating conditions. Higher thermal load under high duty cycle conditions lead to thermal lensing near the optics, as nitrogen's index of refraction experiences a significant change with temperature compared to helium. As such, redesigned LNMs that allow for optimal nitrogen flow have been developed and tested. Initial factory data shows that, using these redesigned LNMs, nitrogen is a viable substitute for helium (see Figure 4).

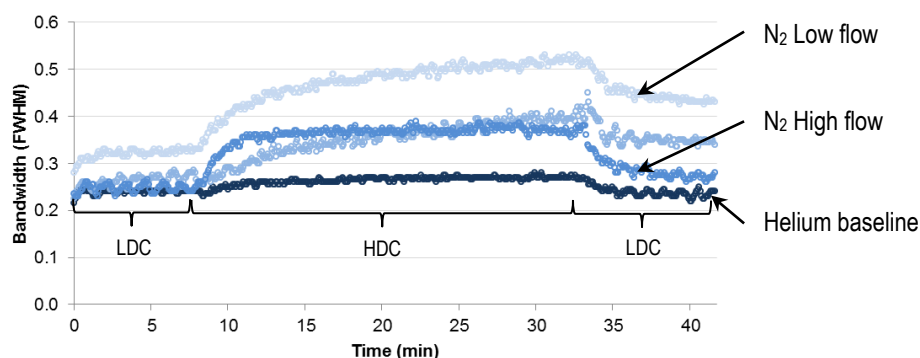


Figure 4. Bandwidth response to nitrogen purge during stress testing

4. NEON REDUCTION SOLUTION

Neon gas is one of the primary consumables of excimer light sources, and its essential role has been described in detail in previous work [3]. Historically, neon gas had been in oversupply and customers have experienced low prices for the past 30 years [4]. However, due to geopolitical instabilities neon supply decreased and price ballooned to historical highs. Cymer released a neon reduction solution to address increased price, limited supply, and higher business continuity risks that its customers experienced [3].

Cymer's neon reduction solution is based on proven, patented GLX technology and has demonstrated reduction for both ArF and KrF light sources while maintaining high availability. GLX technology has helped chipmakers to increase their productivity by reducing gas management events [12]. Improvements to the gas control algorithm in this technology to achieve neon reduction were described in previous work [3].

A comparison between average usage rates of the released solutions across a population of ArF immersion light sources in HVM over a two-year period shows the significant decrease in gas consumption rates (see Figure 5).

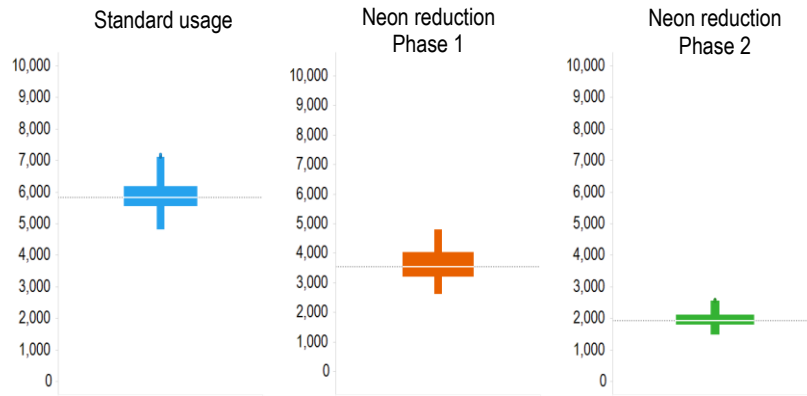


Figure 5. ArF Light source (dual chamber) gas consumption distribution for systems in HVM

Light source gas consumption is dependent on certain operating conditions and shows a distribution about the expected reduction values. The mean consumption value in Liters per Billion pulses (L/Bp) is reduced as well as the upper and lower bounds as described in Table 1. Systems operating with the Phase 2 solution have achieved consumption rates as low as 1,500 L/Bp while maintaining stable performance.

Table 1. ArF Light source gas consumption distribution summary (L/Bp)

	<i>Standard usage</i>	<i>Phase 1</i>	<i>Phase 2</i>
Third Quartile	6,200	4,000	2,100
Median	5,800	3,500	1,900
First Quartile	5,600	3,200	1,800

A neon reduction solution was also implemented for KrF light sources (see Figure 6), which is also based on GLX technology. This solution was developed to restore the high availability that was limited by the containment initially released to provide customers with immediate savings [3].

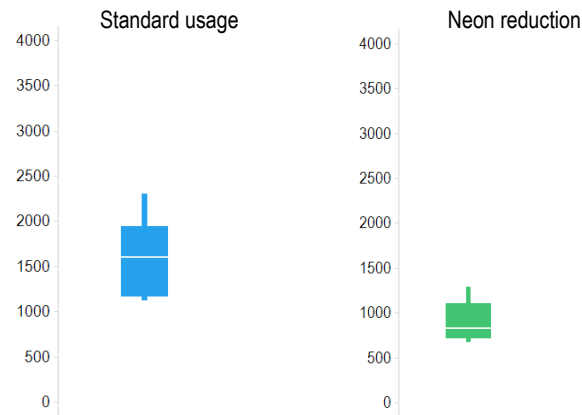


Figure 6. KrF Light source (single chamber) gas consumption trend for systems in HVM

A gas consumption distribution is also expected for KrF systems due to light sources having different firing conditions and operating patterns. Table 2 provides a description of this distribution over a long-term period.

Table 2. Light source gas consumption by neon reduction (L/Bp)

	<i>Standard usage</i>	<i>Neon reduction solution</i>
Third Quartile	1,900	1,100
Median	1,600	800
First Quartile	1,200	700

5. NEON RECYCLE SYSTEM

Cymer is facilitating gas reuse by developing and qualifying a unit to provide in-situ recycling of neon through a sequence of filtering, spectral analysis, and mixture reconstitution. This neon recycle unit allows for >90% of the discharged process gas from the light sources to be purified and reused. The goal is to reduce the overall gas requirements for connected light sources by reducing the overall consumption rate from the baseline before the implementation of the neon reduction solution (see Figure 7).

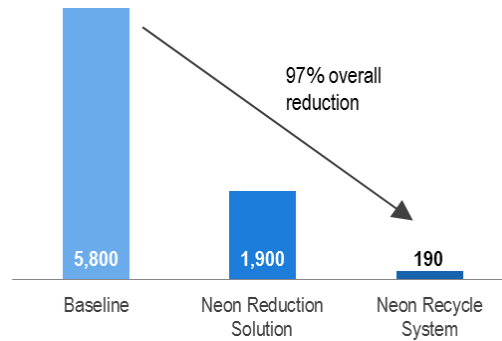


Figure 7. Gas consumption rate (L/Bp) trend for connected systems

The neon recycle unit collects the exhaust gas from the light source after the fluorine has been removed. This fluorine removal occurs inside the light source enclosure and has been an integral safety component since the early models. This exhaust gas is then primarily composed of a mixture of neon, argon, and other minor components. A level of impurities resulting from the discharge inside the chamber are present in this gas and are the primary target of removal by this recycle unit.

The dual stage purification module has a regenerative filter that removes the impurities from the discharge process and has been shown to restore the rare gas mix to purification levels equivalent to ultra-high purity grade (99.999%). The purification module has been shown to maintain consistent and repeatable performance during 6 months of prototype testing.

The gas analyzer module is a key component of the system because it must meet stringent requirements to sample the purified gas with high speed and accuracy. Introducing impurities into the gas supply may degrade laser performance and therefore robust analytical capabilities are required. Additionally, the gas mixture ratios are sampled for compliance against the gas specifications determined by Cymer. The results of this analytical sampling are used in a closed-loop control to determine the required gas additions in the blending portion of the unit.

Once the gas is purified and mixed to the appropriate levels, the recycled mixture is introduced to the bi-mix supply distribution (see Figure 8).

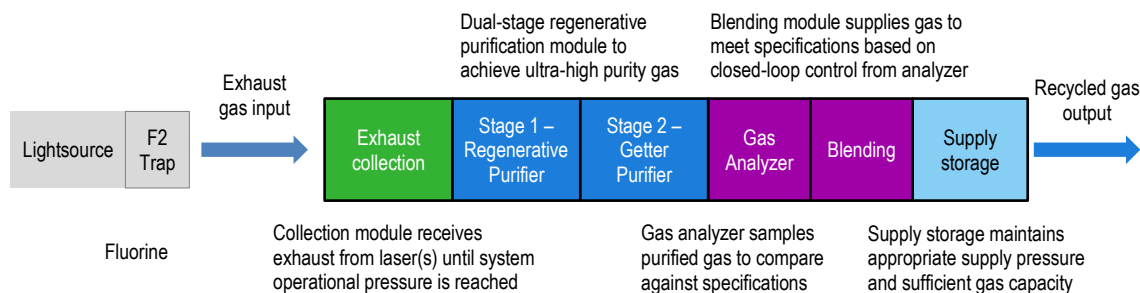


Figure 8. Neon recycle system concept

High-resolution gas analytical capabilities (see Figure 8) allow blend control to maintain recycled gas to ultra-high purity (UHP) specifications. Review of the gas analysis demonstrated that the recycled gas output meets the gas specifications of ArF light sources. Additionally, light source performance was stable and showed no significant difference between facility and recycled gas.

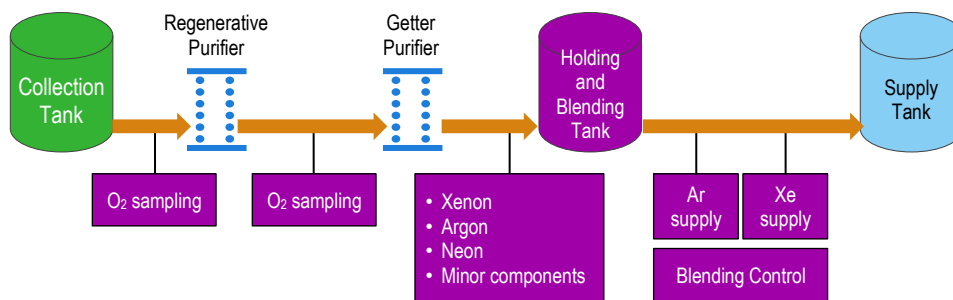


Figure 9. Analytical and blend control schematic

6. CONCLUSION

Cymer's sustainability program has successfully reduced overall light source cost of operation by 50% through reduction initiatives in energy, helium, and neon (see Figure 10). These initiatives are the result of extensive algorithm development, new module designs, and integrated technologies that had a significant impact not only with chipmakers, but also in the global effort to reduce the environmental footprint of semiconductor industry. Cymer will continue to introduce new technologies to reduce the pressure of rising costs, decrease supply continuity risks, and reduce the dependency on non-renewable gases.

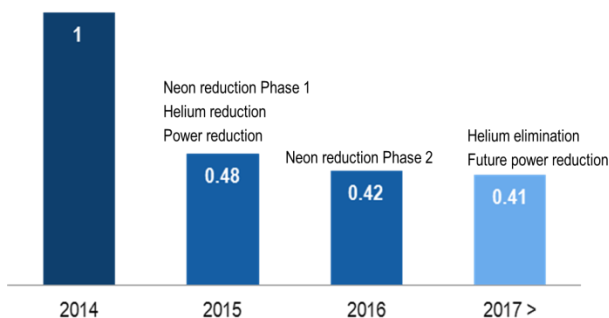


Figure 10. Relative operational cost scale for ArF light sources

7. REFERENCES

- [1] E. Gross, G. G. Padmabandu, R. Ujazdowski, D. Haran and e. a. Matt Lake, "Enabling CoO improvement thru green initiatives," *SPIE - Optical Microlithography XXVIII*, 942626, vol. 9426, 2015.
- [2] D. Brown, P. O'Keeffe, V. Fleurov, R. Rokitski, R. Bergstedt, I. Fomenkov and K. O'Brien, "XLR 500i: Recirculating Ring ArF Light Source for Immersion," *SPIE 6520, Optical Microlithography XX*, vol. 6520, 2007.
- [3] D. Kanawade, Y. Roman, T. Cacouris, J. Thornes and K. OBrien, "Neon Reduction Program on Cymer ArF Light Sources," *SPIE - Optical Microlithography XXIX*, vol. 9780, 2016.
- [4] R. Betzendahl, "Another volatile year for rare gases," Betzendahl Gas Consultants, LLC, 1 December 2016. [Online]. Available: <https://www.gasworld.com/another-volatile-year-for-rare-gases/2011826.article>.
- [5] R. Sandstrom, R. Akins, U. Sengupta, C. Reiser, D. Larson and S. Anderson, "Krypton Fluoride Excimer Laser for Microlithography," *SPIE 1088, Optical/Laser Microlithography II*, vol. 407, 1989.
- [6] Cymer LLC, "Cymer Products," [Online]. Available: <http://www.cymer.com/duv>. [Accessed 2016].
- [7] W. N. Partlo, R. L. Sandstrom, I. V. Fomenkov and P. P. Das, "Low cost of ownership KrF excimer laser using a novel pulse power and chamber configuration," *SPIE 2440, Optical/Laser Microlithography VIII*, vol. 2440, 1995.
- [8] R. Ness, P. Melcher, G. Ferguson and C. Huang, "A decade of solid state pulsed power development at Cymer Inc.," *Power Modulator Symposium, 2004 and 2004 High-Voltage Workshop. Conference Record of the Twenty-Sixth International*, 2004.
- [9] V. B. Fleurov, D. J. I. Colon, D. Brown, P. O'Keeffe and H. Besaucele, "Dual-chamber ultra line-narrowed excimer light source for 193-nm lithography," *SPIE - Optical Microlithography XVI*, vol. 1694, 2003.
- [10] C. Nulman, "Helium – Stable, for the near future," *gasworld magazine*, 04 01 2017.
- [11] R. Healy, "Markets returning to equilibrium – Helium Summit 2.0 review," *gasworld*, 01 11 2016. [Online]. Available: <https://www.gasworld.com/markets-returning-to-equilibrium/2011628.article>. [Accessed 2017].
- [12] W. J. D. R. J. D. B. Kevin O'Brien, "Lithography Line Productivity Impact Using Cymer GLX™ Technology," *Optical Microlithography XXII*, Vols. 7274, 72743N, 2009.